

# SPHRAY: A Smoothed Particle Hydrodynamics Ray Tracer for Radiative Transfer

Gabriel Altay<sup>1</sup>, Rupert A.C. Croft<sup>1</sup>, and Inti Pelupessy<sup>1</sup>

<sup>1</sup> *Carnegie Mellon University, Department of Physics, 5000 Forbes Avenue, Pittsburgh PA 15213, USA*

Accepted 200? ???? ??. Received 2007 ???? ??; in original form 2007 xx

## ABSTRACT

We introduce the publically available code SPHRAY, a Smoothed Particle Hydrodynamics (SPH) ray tracer designed to solve the 3D, time dependent, radiative transfer (RT) equation for cosmological density fields. The SPH nature of SPHRAY makes the incorporation of separate hydrodynamics and gravity solvers very natural. SPHRAY relies on a Monte Carlo (MC) ray tracing scheme that does not interpolate the SPH particles onto a grid but instead integrates directly through the SPH kernels. Given an arbitrary (series of) SPH density field(s) and a description of the sources of ionizing radiation, the code will calculate the non-equilibrium ionization and temperature state of Hydrogen (HI, HII) and Helium (HeI, HeII, HeIII). The sources of radiation can include point like objects, diffuse recombination radiation, and a background field from outside the computational volume. The MC ray tracing implementation allows for the quick introduction of new physics and is parallelization friendly. A quick Axis Aligned Bounding Box (AABB) test taken from computer graphics applications allows for the acceleration of the raytracing component. We present the algorithms used in SPHRAY and verify the code by performing the test problems detailed in the recent Radiative Transfer Comparison Project of Iliev et. al. The source code for SPHRAY and example SPH density fields are made available on a companion website ([www.sphray.org](http://www.sphray.org)).

**Key words:** cosmology, theory, numerical methods, N-body, SPH, ray tracing, Monte Carlo, simulations, radiative transfer, reionization, Strömgren

## 1 INTRODUCTION

In numerical cosmology, prescriptions for the treatment of gravity and hydrodynamics are well developed and have been validated against one another in several comparison studies (see Frenk et al., 1999; O’Shea et al., 2005; Heitmann et al., 2005, 2007; Regan et al., 2007; Agertz et al., 2007; Price, 2007). The density and temperature fields they produce provide input for sub-resolution models of star formation and feedback via supernovae (e.g. Springel & Hernquist, 2003) and black holes (e.g. Di Matteo et al., 2007). Numerical radiative transfer (RT) techniques, necessary to calculate the interaction of the ionizing photons produced by these sources with the cosmological gas, have not yet reached the level of maturity attained by  $N$ -body and gas dynamics solvers. Flexible and accurate RT techniques, validated against analytic solutions and in comparison projects, are necessary to properly interpret many observations and guide the development of theoretical models from cosmological through stellar scales. This is especially true for analy-

sis of upcoming 21 cm surveys such as 21CMA<sup>1</sup> (formerly PAST), LOFAR<sup>2</sup>, MWA<sup>3</sup>, SKA<sup>4</sup>; modeling absorption lines in the spectra of high redshift quasars and gamma ray burst afterglows, and understanding the feedback processes which influence star and galaxy formation.

The introduction of 3D radiative transfer into cosmological simulations is complicated by several issues. The specific intensity  $I_\nu = I(\vec{x}, \hat{n}, \nu, t)$  is a function of seven variables leading to a solution space with high dimensionality. R-type ionization fronts can travel at nearly the speed of light through underdense regions and many times the speed of sound in dense regions leading to radiative time scales orders of magnitude smaller than dynamical time scales. In addition, radiative transfer and hydrodynamic processes are coupled. For example, photo heating creates large pressure gradients near luminous sources and can modify star formation rates while hydrodynamic temperature changes affect

<sup>1</sup> <http://21cma.bao.ac.cn/index.php>

<sup>2</sup> [www.lofar.org](http://www.lofar.org)

<sup>3</sup> [www.haystack.mit.edu/ast/arrays/mwa](http://www.haystack.mit.edu/ast/arrays/mwa)

<sup>4</sup> [www.skatelescope.org](http://www.skatelescope.org)

the recombination, collisional ionization, and radiative cooling rates of the cosmological gas.

In designing a numerical radiative transfer scheme, it is practical to utilize the hydrodynamic frameworks that have already been developed. These can generally be categorized as Lagrangian, particle based methods (see Monaghan, 1992, for a review of Smoothed Particle Hydrodynamics) or Eulerian, grid based methods (see e.g. Norman, 2004, for information on Adaptive Mesh Refinement codes). In this paper, we describe SPHray, a code that performs radiative transfer calculations on Smoothed Particle Hydrodynamics (SPH) density fields. A flexible, general purpose, radiative transfer method tightly coupled to SPH hydrodynamic simulations could be adapted to handle many different astrophysical problems. Currently, SPHray works on static density fields. However, it calculates quantities that are equivalent to the change in specific energy (or entropy) for individual SPH particles due to photoionization/photoheating. This makes the coupling of SPHray with gravity and hydrodynamics relatively straightforward. We leave this to future work.

SPH (Lucy, 1977; Gingold & Monaghan, 1977) is a gridless, Lagrangian method that discretizes a fluid into particles. The self-gravity of these particles can be treated in the same way as  $N$ -Body particles, but they are also subject to hydrodynamic forces. The combination of SPH with tree structures (Hernquist & Katz, 1989) and of tree structures with the particle-mesh method (Xu, 1995; Bagla, 2002), provides a very flexible computational tool.

The earliest combinations of SPH and RT were by Lucy (1977) - one of the papers that introduced SPH - and Brookshaw (1985). These authors modeled radiation transport as a diffusion process. The study of dense astrophysical regions such as molecular clouds and collapsing protostars has continued along this line in the work of Whitehouse & Bate (2004); Whitehouse et al. (2005); Viau et al. (2006) and Mayer et al. (2007).

The highly variable optical depths through voids and Lyman Limit systems in cosmological volumes do not lend themselves to a diffusion description of radiation. Here, either raytracing schemes or moment methods must be used. SPHray uses Monte Carlo ray tracing to accomplish RT. The simplicity of this approach allows new physics to be included in SPHray very easily and provides a framework that is conducive to parallelization. The accuracy of raytracing methods in general is determined by their ability to cover the simulation volume with a sufficient number of rays. This is a computationally expensive process and various approaches have been presented in the literature.

Oxley & Woolfson (2003) combined a raytracing scheme with SPH in which the emitters and absorbers of radiation are at the deepest levels of a Barnes & Hut tree. In this scheme, the internal energies of the SPH particles are modified by interpolating the changes in energy of the tree leaves onto the particles and vice versa. These radiative calculations are made in between hydrodynamic time steps and allow for the coupling of the two processes. Stamatellos & Whitworth (2005) use a similar Barnes & Hut ray tracing scheme, but supplement the radiative transfer cells from the tree with a further star grid around sources.

Both of these methods, in effect, propagate photon packets through a randomly chosen optical depth and then

allow them to be absorbed or scatter. In this way, the temperature and emergent spectra can be calculated, however neither method solves for the ionization fraction explicitly but instead uses either a temperature-opacity or a total density-opacity relation. In addition, they raytrace through the adaptive grids generated from the Barnes & Hut trees and not the SPH particles themselves.

Kessel-Deynet & Burkert (2000), taking advantage of the neighbor lists already in place in SPH simulations, introduced a fast method to find the optical depth from a source to a target particle. Variations of this method have since been utilized in Susa (2006) and Dale et al. (2007) to construct radiative transfer schemes in which each particle influenced by the radiation of a source, becomes a target of that source during the radiative update. A decision concerning how to treat the target particle is made based on the optical depth along the ray connecting the source and the target. Yoshida et al. (2007) have presented a related method in which photon arrival times are calculated for each particle surrounding a given source by integrating the ionization front jump conditions along rays. After the photon arrival time for a source-particle pair, the photoionization rate is computed in the optically thin limit. Pawlik & Schaye (2008) have recently introduced an SPH / photon packet based radiative transfer scheme in which packets are emitted into cones around the sources and propagated among the particles using the neighbor search lists.

SPHray differs from the above methods in that it first uses a fast Axis Aligned Bounding Box (AABB) test to find the intersections of a ray and a Barnes & Hut tree that stores the particles. Next, the particles in these tree leaves are tested to see if they intersect the ray, yielding their impact parameter. In this way, every particle whose smoothing volume is intersected by the ray is stored in a raylist. In the course of moving along the ray from the source, the ionization and temperature state of each particle is updated leading to more particle updates per ray. In this sense, SPHray shares the same ray-update ideas as the Monte Carlo ray tracing code CRASH by Maselli et al. (2003), but is applied to SPH density fields. With a sufficient number of rays, the native SPH resolution can be preserved.

The format of this paper is as follows. In §2 we review the basic equations governing radiative transport and the evolution of the ionization and temperature state of a cosmological gas. We also derive approximate analytic solutions necessary for an iterative numerical solution. In §3 we describe the algorithms used by SPHray. In §4 we present the results of several standard RT tests. These tests were chosen to be the same as those in a recent radiative transfer comparison project (Iliev et al., 2006). They include: (1) isothermal HII region expansion; (2) HII region expansion with evolving temperature; (3) I-front trapping and shadowing by a dense clump; (4) multiple sources in a cosmological density field. We make our closest comparisons of SPHray with CRASH (the only other Monte Carlo code in the project), and a code described in Susa (2006) called RSPH (the only other SPH code in the project). Finally, in §5 we discuss future applications and improvements of SPHray as well as summarizing and discussing our results.

## 2 BASIC PHYSICS - RADIATIVE TRANSFER, IONIZATION, AND TEMPERATURE EVOLUTION

In this section we review the equations of 3D radiative transfer, the ionization and temperature equations for a cosmological gas, and the approximations that are made in SPHRAY. To facilitate comparison with other radiative transfer codes we review some of the other approximations which can be made.

### 2.1 Notation

In what follows, we use Roman numerals to indicate the ionization state of an element (H,He) in the standard way. Elements without Roman numerals refer to the nuclei of atoms (or all ionization states). A subscripted  $n$  refers to the number density of an element (or a specific ionization state of an element). A subscripted  $x$  refers to the ratio of the number density of a specific ionization state to the number density of all nuclei of that element. A subscripted  $y$  refers to the ratio of the number density of the subscripted species to the number density of H nuclei, for example,

$$x_{\text{HeII}} = \frac{n_{\text{HeII}}}{n_{\text{He}}} \quad (1)$$

$$y_{\text{HeIII}} = \frac{n_{\text{HeIII}}}{n_{\text{H}}} \quad (2)$$

### 2.2 Radiative Transfer Equation

The 3-D radiative transfer equation in a frame comoving with the expansion of the Universe can be written (e.g. Norman et al., 1998),

$$\frac{1}{c} \frac{\partial I_\nu}{\partial t} + \frac{\hat{\mathbf{n}} \cdot \nabla I_\nu}{\bar{a}} - \frac{H}{c} \left( \nu \frac{\partial I_\nu}{\partial \nu} - 3I_\nu \right) = \epsilon_\nu - \kappa_\nu I_\nu \quad (3)$$

where  $\epsilon_\nu$  and  $\kappa_\nu$  are the emission and extinction coefficients respectively,  $H = \dot{a}/a$  is the Hubble parameter,  $\bar{a} = a/a_e$  is the scale factor at time  $t$  divided by the scale factor at time  $t_e$  (when the photons in the ray were emitted), and  $I_\nu = I(\vec{x}, \hat{\mathbf{n}}, \nu, t)$  is the specific intensity.

For photons with a mean free path  $\lambda_{\text{mfp}}$  much less than the Horizon size  $c/H$ , the classical radiative transfer equation is a valid approximation.

$$\frac{1}{c} \frac{\partial I_\nu}{\partial t} + \hat{\mathbf{n}} \cdot \nabla I_\nu = \epsilon_\nu - \kappa_\nu I_\nu \quad (4)$$

This local approximation holds fairly well before the percolation stage of reionization when the growing ionization bubbles are still insulated from each other by the optically thick IGM. Care must be taken once the majority of the IGM is reionized and becomes optically thin allowing photons to travel distances greater than the simulation box length. The effect of these background fluxes from outside the simulation volume must be taken into account, especially for high energy photons which have longer mean free paths and the potential to ionize and heat the IGM after being redshifted. The treatment of these non-local fluxes should be tailored to the specific problem at hand and so were not 'hard-wired' into SPHRAY. For the test cases presented in §4 they were not necessary.

Another caveat to using the classical equation, as explained in Abel et al. (1999), is that it is only valid when  $|\nu \partial I_\nu / \partial \nu| \leq I_\nu$  and hence only for continuum radiation. However, the classical equation can still be used for line radiation if the redshifted absorption (photo-ionization) cross-sections are used when determining  $\kappa_\nu$ .

If  $\epsilon_\nu$  and  $\kappa_\nu$  can be approximated as constant, a time independent RT equation can be used.

$$\hat{\mathbf{n}} \cdot \nabla I_\nu = \epsilon_\nu - \kappa_\nu I_\nu \quad (5)$$

This is a good approximation for individual SPH particles over a sufficiently short time, however (as is also discussed in Abel et al., 1999) it breaks down close to sources and allows the possibility of ionization fronts that travel faster than the speed of light. This can be quantified by examining the ionization front jump condition for a single point source ionizing a uniform density, constant temperature, Hydrogen gas,

$$n_{\text{H}} \frac{dr_I}{dt} = \frac{\dot{N}}{4\pi r_I^2} - \alpha_{\text{H}} \int_0^{r_I} n_e n_{\text{H}} x_{\text{HII}} dr \quad (6)$$

where,  $r_I$  is the distance to the ionization front from the source,  $\dot{N}$  is the number of photons per second emitted by the source, and  $\alpha_{\text{H}}$  is the recombination rate. An upper limit on the radius,  $r_c$  within which the ionization front has a speed greater than  $c$  is,

$$r_c \leq \sqrt{\frac{\dot{N}}{4\pi n_{\text{H}} c}}. \quad (7)$$

Within this region, use of the time independent equation breaks down. In a raytracing scheme, this can be avoided by stopping rays once they have reached a distance  $d = ct_{\text{on}}$  where  $t_{\text{on}}$  is the amount of time the source has been on. The photons that were in the ray can be saved and traced from the stopping point once enough time has elapsed. In practice this is not always necessary. For example, the first test presented in §4 has  $r_c/r_s = 6.9 \times 10^{-3}$  where the Strömgen radius,  $r_s = 5.4$  kpc,

In SPHRAY, the diffuse component of the radiation field is modeled using the on-the-spot (OTS) approximation, or as a set of many point sources and so for all calculations we can set  $\epsilon_\nu = 0$  along the ray, further simplifying the RT equation,

$$\frac{\partial I_\nu}{\partial r} = -\kappa_\nu I_\nu \quad (8)$$

which has the analytic solution,

$$I_\nu(r) = I_\nu(r_0) e^{-\tau(r)} \quad (9)$$

where

$$\tau = \int_0^r n_x(r) \sigma(\nu) dr = \int_0^r \kappa_\nu dr \quad (10)$$

In principle,  $\kappa_\nu$  should include contributions from every process that removes photons from the ray under consideration (photo absorption, Thomson scattering, dust, etc.). For the tests presented here, we consider only photo absorption, however it would be straightforward to add terms to account for other processes.

### 2.3 Ionization Equations

In this section we review the equations that determine the time development of the ionization fractions. They represent the contributions from photo-ionization, collisional ionization and recombination. Analytic and time averaged solutions in the case of constant rates are derived for use in an iterative solution scheme which relaxes the stringent constraints on the time step.

#### 2.3.1 Chemistry

SPHRAY follows the non-equilibrium evolution of six species  $[x_{\text{HI}}, x_{\text{HII}}, x_{\text{HeI}}, x_{\text{HeII}}, x_{\text{HeIII}}, y_e]$ , only three of which are independent.

$$x_{\text{HI}} + x_{\text{HII}} = 1 \quad (11)$$

$$x_{\text{HeI}} + x_{\text{HeII}} + x_{\text{HeIII}} = 1 \quad (12)$$

$$y_e = y_{\text{HII}} + y_{\text{HeII}} + 2y_{\text{HeIII}} + y_z \quad (13)$$

where  $y_z$  represents a constant background of free electrons from ionized metals. This background has a negligible effect on the evolution of the ionization fractions of H and He, but provides stability in the case of very small levels of ionization. We note that this is a subset of all atomic species relevant to primordial chemistry. Although inclusion of species involved in the formation of molecular Hydrogen  $[\text{H}^-, \text{H}_2, \text{H}_2^+]$  is important in studies of primordial star formation, they have only a small impact on the evolution of the IGM. Primordial gas chemistry is discussed in detail in Anninos et al. (1997) and Abel et al. (1997).

#### 2.3.2 Differential Equations

The processes that we will consider in the evolution of the ionization fractions are, recombination  $\alpha_I$ , collisional ionization  $\gamma_A$ , and photo-ionization  $\Gamma_A$  where  $A \in \{\text{HI}, \text{HeI}, \text{HeII}\}$  is one of the photo absorbing species and  $I \in \{\text{HII}, \text{HeII}, \text{HeIII}\}$  is one of the photo-ionized species. The equations can be written down directly,

$$\frac{dx_{\text{HI}}}{dt} = -G_{\text{HI}}x_{\text{HI}} + R_{\text{HII}}x_{\text{HII}} \quad (14)$$

$$\frac{dx_{\text{HII}}}{dt} = G_{\text{HI}}x_{\text{HI}} - R_{\text{HII}}x_{\text{HII}} \quad (15)$$

$$\frac{dx_{\text{HeI}}}{dt} = -G_{\text{HeI}}x_{\text{HeI}} + R_{\text{HeII}}x_{\text{HeII}} \quad (16)$$

$$\frac{dx_{\text{HeII}}}{dt} = G_{\text{HeI}}x_{\text{HeI}} - (G_{\text{HeII}} + R_{\text{HeII}})x_{\text{HeII}} + R_{\text{HeIII}}x_{\text{HeIII}} \quad (17)$$

$$\frac{dx_{\text{HeIII}}}{dt} = G_{\text{HeII}}x_{\text{HeII}} - R_{\text{HeIII}}x_{\text{HeIII}} \quad (18)$$

where we have grouped the ionizing terms ( writing  $G_A = \Gamma_A + \gamma_A n_e$ ) together, and included the electron number density in the recombination term ( $R_I = \alpha_I n_e$ ). In matrix form,

$$\dot{\mathbf{x}}_{\text{H}} = \mathbf{M}_{\text{H}}\mathbf{x}_{\text{H}} \quad (19)$$

$$\dot{\mathbf{x}}_{\text{He}} = \mathbf{M}_{\text{He}}\mathbf{x}_{\text{He}} \quad (20)$$

where,

$$\mathbf{M}_{\text{H}} = \begin{pmatrix} -G_{\text{HI}} & R_{\text{HII}} \\ G_{\text{HI}} & -R_{\text{HII}} \end{pmatrix} \quad (21)$$

$$\mathbf{M}_{\text{He}} = \begin{pmatrix} -G_{\text{HeI}} & R_{\text{HeII}} & 0 \\ G_{\text{HeI}} & -(G_{\text{HeII}} + R_{\text{HeII}}) & R_{\text{HeIII}} \\ 0 & G_{\text{HeII}} & -R_{\text{HeIII}} \end{pmatrix} \quad (22)$$

In general, every species with  $N_{\text{is}}$  ionization states leads to an  $N_{\text{is}} \times N_{\text{is}}$  tridiagonal matrix.

#### 2.3.3 Analytic Solutions

In order to proceed with a straightforward numerical integration, the equations in the previous section are sufficient. However, the time steps are restricted by the stiff nature of the differential equations and so SPHRAY can also be run with an iterative ionization solver. This solver is based on the method used in the code C<sup>2</sup>-Ray presented by Mellema et al. (2006) where the detailed Hydrogen solution is given. For completeness we give the Helium solutions as well. The specific implementation in SPHRAY is described in §3. It requires time averaged analytic solutions for the ionization fractions which are derived below.

If we assume that the  $G_A$  and  $R_I$  are constant the analytic solutions have the following form,

$$x_{\text{HI}}(t) = x_{\text{HI}}^{eq} + C_{\text{H}}^1 e^{\nu t} \quad (23)$$

$$x_{\text{HII}}(t) = x_{\text{HII}}^{eq} + C_{\text{H}}^2 e^{\nu t} \quad (24)$$

$$x_{\text{HeI}}(t) = x_{\text{HeI}}^{eq} + C_{\text{He}}^1 e^{\lambda_1 t} + C_{\text{He}}^2 e^{\lambda_2 t} \quad (25)$$

$$x_{\text{HeII}}(t) = x_{\text{HeII}}^{eq} + C_{\text{He}}^3 e^{\lambda_1 t} + C_{\text{He}}^4 e^{\lambda_2 t} \quad (26)$$

$$x_{\text{HeIII}}(t) = x_{\text{HeIII}}^{eq} + C_{\text{He}}^5 e^{\lambda_1 t} + C_{\text{He}}^6 e^{\lambda_2 t} \quad (27)$$

with the equilibrium solutions given by,

$$x_{\text{HI}}^{eq} = \frac{R_{\text{HII}}}{G_{\text{HI}} + R_{\text{HII}}} \quad (28)$$

$$x_{\text{HII}}^{eq} = \frac{G_{\text{HI}}}{G_{\text{HI}} + R_{\text{HII}}} \quad (29)$$

$$x_{\text{HeI}}^{eq} = \frac{R_{\text{HeII}}R_{\text{HeIII}}}{R_{\text{HeII}}R_{\text{HeIII}} + R_{\text{HeII}}G_{\text{HeI}} + G_{\text{HeI}}G_{\text{HeII}}} \quad (30)$$

$$x_{\text{HeII}}^{eq} = \frac{R_{\text{HeIII}}G_{\text{HeI}}}{R_{\text{HeII}}R_{\text{HeIII}} + R_{\text{HeII}}G_{\text{HeI}} + G_{\text{HeI}}G_{\text{HeII}}} \quad (31)$$

$$x_{\text{HeIII}}^{eq} = \frac{G_{\text{HeI}}G_{\text{HeII}}}{R_{\text{HeII}}R_{\text{HeIII}} + R_{\text{HeII}}G_{\text{HeI}} + G_{\text{HeI}}G_{\text{HeII}}} \quad (32)$$

Each system has one eigenvalue equal to zero corresponding to the equilibrium solutions. The non-zero eigenvalues and the other constants can be expressed in terms of the  $G_A$  and  $R_I$ . For Hydrogen,

$$C_{\text{H}}^1 = \Delta x_{\text{HI}} = x_{\text{HI}}^0 - x_{\text{HI}}^{eq} \quad (33)$$

$$C_{\text{H}}^2 = \Delta x_{\text{HII}} = x_{\text{HII}}^0 - x_{\text{HII}}^{eq} \quad (34)$$

$$\nu = -(G_{\text{HI}} + R_{\text{HII}}) \quad (35)$$

$$\nu = -(G_{\text{HI}} + R_{\text{HII}}) \quad (36)$$

where  $x_{\text{HI}}^0$  and  $x_{\text{HeII}}^0$  are initial values and  $\nu$  is the non-zero eigenvalue for the Hydrogen system. For Helium, the expressions contain more terms, but they can be easily written down with the use of some notation. The matrix  $\mathbf{S}_{\text{He}}$  of eigenvectors that will diagonalize  $\mathbf{M}_{\text{He}}$  is,

$$\mathbf{S}_{\text{He}} = \mathbf{S}_{\text{He}}^{i,j} = \begin{pmatrix} \frac{R_{\text{HeII}}}{G_{\text{HeI}}} & \frac{R_{\text{HeII}}}{\lambda_1 + G_{\text{HeI}}} & \frac{R_{\text{HeII}}}{\lambda_2 + G_{\text{HeI}}} \\ 1 & 1 & 1 \\ \frac{G_{\text{HeII}}}{R_{\text{HeIII}}} & \frac{G_{\text{HeII}}}{\lambda_1 + R_{\text{HeIII}}} & \frac{G_{\text{HeII}}}{\lambda_2 + R_{\text{HeIII}}} \end{pmatrix} \quad (37)$$

where  $\lambda_1$  and  $\lambda_2$  are the non-zero eigenvalues of the Helium system.

$$\lambda_1 = -(s + p) \quad (38)$$

$$\lambda_2 = -(s - p) \quad (39)$$

with

$$s = \frac{1}{2}(R_{\text{HeII}} + R_{\text{HeIII}} + G_{\text{HeI}} + G_{\text{HeII}}) \quad (40)$$

$$d = R_{\text{HeII}}R_{\text{HeIII}} + R_{\text{HeIII}}G_{\text{HeI}} + G_{\text{HeI}}G_{\text{HeII}} \quad (41)$$

$$p = \sqrt{s^2 - d} \quad (42)$$

We require the six constants  $C_{\text{He}}^i$  in terms of the values  $G_A$  and  $R_I$ . Because the Helium system is constrained by the three differential equations and the fact that the ionization fractions must sum to one, there is some choice in the way we do this. SPHRAy follows  $x_{\text{HeII}}$  and  $x_{\text{HeIII}}$  and so a convenient relation is,

$$C_{\text{He}}^1 = b\mathbf{S}_{\text{He}}^{1,2} \quad C_{\text{He}}^3 = b \quad C_{\text{He}}^5 = b\mathbf{S}_{\text{He}}^{3,2} \quad (43)$$

$$C_{\text{He}}^2 = c\mathbf{S}_{\text{He}}^{1,3} \quad C_{\text{He}}^4 = c \quad C_{\text{He}}^6 = c\mathbf{S}_{\text{He}}^{3,3} \quad (44)$$

with,

$$b = \frac{\Delta x_{\text{HeIII}} - \Delta x_{\text{HeII}}\mathbf{S}_{\text{He}}^{3,3}}{\mathbf{S}_{\text{He}}^{3,2} - \mathbf{S}_{\text{He}}^{3,3}} \quad (45)$$

$$c = \frac{\Delta x_{\text{HeII}}\mathbf{S}_{\text{He}}^{3,2} - \Delta x_{\text{HeIII}}}{\mathbf{S}_{\text{He}}^{3,2} - \mathbf{S}_{\text{He}}^{3,3}} \quad (46)$$

At the heart of this iterative method is the use of time averaged ionization fractions, optical depths, and photo-ionization rates to take larger time steps than would normally be possible. The time averaged ionization fractions  $\langle x \rangle = \frac{1}{\Delta t} \int_0^{\Delta t} x(t)dt$  of the above solutions are,

$$\langle x_{\text{HI}} \rangle = x_{\text{HI}}^{eq} + \frac{C_{\text{H}}^1}{\nu} (e^{\nu\Delta t} - 1) \frac{1}{\Delta t} \quad (47)$$

$$\langle x_{\text{HII}} \rangle = x_{\text{HII}}^{eq} + \frac{C_{\text{H}}^2}{\nu} (e^{\nu\Delta t} - 1) \frac{1}{\Delta t}. \quad (48)$$

$$\langle x_{\text{HeI}} \rangle = x_{\text{HeI}}^{eq} +$$

$$\left[ \frac{C_{\text{He}}^1 (e^{\lambda_1\Delta t} - 1)}{\lambda_1\Delta t} + \frac{C_{\text{He}}^2 (e^{\lambda_2\Delta t} - 1)}{\lambda_2\Delta t} \right] \quad (49)$$

$$\langle x_{\text{HeII}} \rangle = x_{\text{HeII}}^{eq} +$$

$$\left[ \frac{C_{\text{He}}^3 (e^{\lambda_1\Delta t} - 1)}{\lambda_1\Delta t} + \frac{C_{\text{He}}^4 (e^{\lambda_2\Delta t} - 1)}{\lambda_2\Delta t} \right] \quad (50)$$

$$\langle x_{\text{HeIII}} \rangle = x_{\text{HeIII}}^{eq} +$$

$$\left[ \frac{C_{\text{He}}^5 (e^{\lambda_1\Delta t} - 1)}{\lambda_1\Delta t} + \frac{C_{\text{He}}^6 (e^{\lambda_2\Delta t} - 1)}{\lambda_2\Delta t} \right] \quad (51)$$

## 2.4 Temperature Equation

There are three terms in the temperature evolution equation. One for the photo heating  $\mathcal{H}$ , one for various atomic cooling<sup>5</sup> processes  $\Lambda$ , and one for the change in temperature due to the change in the number of free particles.

$$\frac{dT}{dt} = \frac{2}{3nk_B}(\mathcal{H} - \Lambda) - \frac{T}{n} \frac{dn}{dt} \quad (52)$$

### 2.4.1 Photo Heating Term

The term  $\mathcal{H}$  accounts for the kinetic energy of the photoionized electrons which quickly gets transferred to the other particle species. Let us suppose that a unit volume of gas absorbs  $\dot{N}_\gamma$  photons per second. The fraction of absorption due to a given particle species is proportional to the optical depth of that species through the volume. The photo-heating rate for a monochromatic ray,  $\mathcal{H} = \mathcal{H}_{\text{HI}} + \mathcal{H}_{\text{HeI}} + \mathcal{H}_{\text{HeII}}$  can be simply expressed in this way,

$$\mathcal{H}_{\text{HI}} = \dot{N}_\gamma \frac{\tau_{\text{HI}}}{\tau_{\text{all}}} (h\nu - h\nu_{\text{HI}}) \quad (53)$$

$$\mathcal{H}_{\text{HeI}} = \dot{N}_\gamma \frac{\tau_{\text{HeI}}}{\tau_{\text{all}}} (h\nu - h\nu_{\text{HeI}}) \quad (54)$$

$$\mathcal{H}_{\text{HeII}} = \dot{N}_\gamma \frac{\tau_{\text{HeII}}}{\tau_{\text{all}}} (h\nu - h\nu_{\text{HeII}}) \quad (55)$$

where  $\nu_{\text{HI}}$ ,  $\nu_{\text{HeI}}$ , and  $\nu_{\text{HeII}}$  are the ionization threshold frequencies.

### 2.4.2 Atomic Cooling Term

The atomic cooling function,  $\Lambda$ , includes the following physical processes,

- Collisional Ionization Cooling (  $\zeta$  )
- Collisional Excitation Cooling (  $\psi$  )
- Recombination Cooling (  $\eta$  )
- Bremsstrahlung Cooling (  $\beta$  )
- Compton Heating/Cooling (  $\chi$  )

The numerical value of  $\Lambda = \Lambda(n_A, n_I, n_e, T, T_{\text{bgnd}})$  is calculated using the rates detailed in Appendix A.

## 3 NUMERICAL TECHNIQUES

In this section we outline the numerical techniques used to solve for the ionization and temperature state. SPHRAy is a Monte Carlo code and is based on sampling the radiation field along 1-d characteristics. This is accomplished by tracing rays that extend a predefined length. The length can be chosen in a number of ways. For vacuum boundary conditions the obvious choice is to terminate the rays at the edge

<sup>5</sup> note that Compton scattering can have a negative contribution to the cooling function if the temperature of the background radiation field is greater than the gas kinetic temperature

of the volume. For reflective or periodic boundary conditions a criterion can be applied to the properties of photons in the ray (for example when the flux has dropped below a specified value) or a hard limit on the length of a ray can be set (for example 2 box lengths). The impact parameter for every particle-ray intersection is calculated using a fast AABB test allowing for the calculation of the photon flux at all the particle-ray intersections.

### 3.1 Sources

Any point in the simulation volume can be specified as the beginning of a ray. Currently, SPHray is configured to treat point sources whose properties are specified by an input file, recombination rays from ionized SPH particles, and background fluxes by specifying points on the simulation volume walls as sources.

#### 3.1.1 Diffuse Recombination Radiation

Here we review the recombination processes that produce ionizing photons in a H/He gas (e.g., Osterbrock, 1989). The following free-bound transitions produce continuous spectra.

$$\text{HII} + e \rightarrow \text{HI}(1^2\text{S}) + \gamma \quad (\approx 13.6 \text{ eV}) \quad (56)$$

$$\text{HeII} + e \rightarrow \text{HeI}(1^1\text{S}) + \gamma \quad (\approx 24.6 \text{ eV}) \quad (57)$$

$$\text{HeIII} + e \rightarrow \text{HeII}(2^2\text{S}) + \gamma \quad (\approx 13.6 \text{ eV}) \quad (58)$$

$$\text{HeIII} + e \rightarrow \text{HeII}(2^2\text{P}) + \gamma \quad (\approx 13.6 \text{ eV}) \quad (59)$$

$$\text{HeIII} + e \rightarrow \text{HeII}(1^2\text{S}) + \gamma \quad (\approx 54.4 \text{ eV}) \quad (60)$$

These spectra can be calculated exactly using the Milne relations. For Hydrogen, the emission coefficient for the above process is (Osterbrock, 1989),

$$\epsilon_{\text{H}}^1 = \frac{2h\nu^3}{c^2} \left( \frac{h^2}{2\pi m_e k_B T} \right)^{3/2} \sigma_{\text{H}}^1 e^{-h(\nu - \nu_{\text{HI}})/k_B T} n_{\text{HII}} n_e \quad (61)$$

where  $\sigma_{\text{H}}^1$  is the photo absorption coefficient of Hydrogen in the ground state. Similar relations can be derived for the other free-bound processes, however in practice these highly peaked spectra can be approximated by delta functions just above the appropriate threshold <sup>6</sup> (in parentheses in the equations above).

Following free-bound captures to excited Helium states, the following bound-bound transitions can also produce ionizing photons.

$$\text{HeI}(2^3\text{S}) \rightarrow \text{HeI}(1^1\text{S}) + \gamma \quad 19.8 \text{ eV} \quad (62)$$

$$\text{HeI}(2^1\text{P}) \rightarrow \text{HeI}(1^1\text{S}) + \gamma \quad 21.2 \text{ eV} \quad (63)$$

$$\text{HeI}(2^1\text{S}) \rightarrow \text{HeI}(1^1\text{S}) + 2\gamma \quad \Sigma 20.6 \text{ eV} \quad (64)$$

$$\text{HeII}(2^2\text{P}) \rightarrow \text{HeII}(1^2\text{S}) + \gamma \quad 40.8 \text{ eV} \quad (65)$$

$$\text{HeII}(2^2\text{S}) \rightarrow \text{HeII}(1^2\text{S}) + 2\gamma \quad \Sigma 40.8 \text{ eV} \quad (66)$$

The various bound-bound transitions above have relative probabilities that depend on the environment (free electron density, temperature, ionization state) and so the weights to

give to these processes should be tailored to specific applications.

The most straight forward way to deal with this diffuse radiation is to use the on-the-spot (OTS) approximation. The OTS approximation makes the assumption that recombination photons are absorbed in the vicinity (the same SPH particle) of the point where they are emitted. Computationally, this means no ray tracing is necessary for these photons. For pure Hydrogen simulations, the OTS approximation amounts to using the reduced recombination rates in the appendix (case B) <sup>7</sup>. Here, one is making the assumption that each electron capture directly to the ground state produces a photon that ionizes a nearby Hydrogen atom and the two actions effectively cancel one another.

For simulations involving Helium, using the case B rates would be making the assumption that each HeII recombination to the ground state ionizes a nearby HeI atom while each HeIII recombination to the ground state ionizes a nearby HeII atom. This is a simple first approximation, but some of the HeII ground state captures will ionize HI, while some of the HeIII ground state captures will ionize HI and HeI. To account for this would require a more detailed adjustment of the recombination and photoionization rates for the species involved. The most computationally intensive option is to trace rays for each of these recombination processes and thereby take account of the fact that some of the photons will not be absorbed in the SPH particle where they were created. Again, the level of detail used should be guided by the application at hand. With SPHray it is possible to choose either the recombination ray or the OTS approach. We plan to explore the accuracy of the OTS approximation in various geometries and densities in future work.

### 3.2 Optical Depth in SPH

Ray tracing solutions to the radiative transfer problem solve the equation along 1D characteristics. As such, an estimate of the optical depth along these characteristics is central to the problem. In the SPH formalism, a continuous density field is represented by a number of discrete fluid elements (particles) with smoothing lengths  $h_i$ . These smoothing lengths <sup>8</sup> are usually defined to keep a constant mass  $M_{\text{sph}}$  inside the smoothing volume  $V_i = \frac{4}{3}\pi h_i^3$ . The properties of the fluid at any point are then estimated by averaging over all  $N$  particles in the simulation weighted by a smoothing kernel. In practice, one only averages over nearby particles, but this definition is equally valid and useful in the derivation to follow. As an example, the density  $\rho(\mathbf{r}_i)$  at the position  $\mathbf{r}_i$  of the  $i^{\text{th}}$  particle is estimated as,

$$\rho(\mathbf{r}_i) \approx \sum_{j=1}^N m_j W(|\mathbf{r}_i - \mathbf{r}_j|, h) = \sum_{j=1}^N m_j W(r_{ij}, h) \quad (67)$$

where  $m_j$  is the mass of the  $j^{\text{th}}$  nearest particle and  $W(r_{ij}, h)$  is a smoothing kernel.

<sup>6</sup> It is a coincidence that electron captures by HeIII directly to the n=2 level of HeII have a spectrum peaked at the Hydrogen threshold.

<sup>7</sup> Case A rates refer to recombinations to all atomic levels. Case B rates refer to recombinations to all but the first atomic level so that  $\alpha_{\text{H}}^1 = \alpha_{\text{H}}^A - \alpha_{\text{H}}^B$ .

<sup>8</sup> Throughout this work we use the convention that the smoothing kernel goes to zero at  $h$  and not  $2h$

An estimate of the fluid property need not be made at the position of a particle. An averaged value for any fluid property can be defined for an arbitrary point in space using two techniques. One is the “scatter” method in which the desired quantity is calculated by averaging over every particle whose smoothing volume includes the point in question.

$$\rho(\mathbf{r}_i) \approx \sum_{j=1}^N m_j W(r_{ij}, h_j) \quad (68)$$

For this case, a different smoothing length  $h_j$  is used in the kernel  $W$  for each term. In the “gather” method, a smoothing length is defined for the arbitrary point and the desired quantity is calculated as an average over the particles within this smoothing length.

$$\rho(\mathbf{r}_i) \approx \sum_{j=1}^N m_j W(r_{ij}, h_i) \quad (69)$$

For this case, only one smoothing length  $h_i$  is involved. For definiteness, a popular spline kernel (Monaghan and Latanzio 1985) is,

$$W(r, h) = \frac{8}{\pi h^3} \begin{cases} 1 - 6(\frac{r}{h})^2 + 6(\frac{r}{h})^3 & 0 \leq r \leq \frac{h}{2} \\ 2(1 - \frac{r}{h})^3 & \frac{h}{2} < r \leq h \\ 0 & r > h \end{cases} \quad (70)$$

In our ray tracing scheme, we would like an estimate of the column depth  $N_{\text{cd}}$  along a ray that has intersected a number of SPH particles. Formally this is,

$$N_{\text{cd}} = \int_0^L \rho(\mathbf{r}) dl \approx \int_0^L \sum_{j=1}^N m_j W(r_{lj}, h_j) dl \quad (71)$$

where the scatter interpretation has been used. The summation extends over all particles and  $l$  parameterizes the distance along the ray. Interchanging the order of integration and summation we have,

$$N_{\text{cd}} \approx \sum_{j=1}^N \int_0^L m_j W(r_{lj}, h_j) dl \quad (72)$$

This amounts to a line integral through the smoothing kernel of each particle whose smoothing volume is pierced by the ray. This integral is calculated by tabulating it as a function of impact parameter  $b$  for one value of  $h$ , namely  $h = 1$ . We can recover the line integral for any  $b$  and  $h$  through a rescaling of the tabulated value. This technique delivers the optical depth to a point along the ray, as well as the contribution from each particle in the raylist to that optical depth.

There are two related approximations that come into play here. The first involves the reordering of the terms so that those involving the same particle are adjacent. This is valid as long as the density doesn’t vary much within a smoothing length which is true by construction. The next involves the endpoint of the ray. Given this reordering, the contribution to the density (at the terminus of the ray) from particles which have centers further down the ray but smoothing volumes that contain the end point, will be unaccounted for. This is a small correction for the reason given above, and the fact that the photons are usually nearly all absorbed when the ray is terminated.

### 3.3 Photon Packets

In our Monte Carlo method, the radiation field is discretized into photon packets and transported along rays. Each packet contains a large number of monochromatic photons sampled from an arbitrary spectral energy distribution (SED). The direction along which a photon packet is transported is also sampled from an emission profile distribution. This is true whether the packet represents emission from a point source, diffuse recombination emission, or background radiation originating outside the computational volume. The starting locations for rays can be any point within the computational volume including points on the faces of the simulation volume.

For each ray that is cast, a source is selected at random weighted by its luminosity. This ensures a population of photon packets with roughly the same energy as opposed to the same number of photon packets being traced from each source regardless of their luminosities.

The base resolution of a simulation is determined by how many SPH particles  $N_p$  are used to sample the continuous density field. The degree to which the sampling of the radiation field approaches the base resolution is determined by the number of rays traced  $N_r$ . For isotropic sources and homogeneous density fields, the average number of particle intersections per ray is  $\approx N_p^{1/3}$ . It follows that the total number of intersections is on the order of  $N_r N_p^{1/3}$  and that the average number of intersections per particle is  $N_r N_p^{-2/3}$ . This gives a rough estimate of how many times the radiation field is sampled at each particle. In practice, particles closer to sources will be sampled more often and it is better to conduct a convergence study than to rely on pre-calculated estimates of resolution.

### 3.4 Particle-Ray Intersections

Once a photon packet has been constructed, it is propagated along a ray. SPHRAY uses a data object called a raylist to store the intersections of a ray drawn from the source, and all the SPH particles whose smoothing volumes are pierced by the ray. This can be done using vacuum, or periodic boundary conditions (in the latter case a maximum length must be specified). The search for these intersections needs to be as efficient as possible.

Because the smoothing lengths within a cosmological box can vary by more than three orders of magnitude, we organize the particles into an oct-tree. This manner of storing particles is common and many SPH codes produce an oct-tree during the course of hydrodynamic calculations. Our code could be trivially modified to use a pre-constructed tree although currently SPHRAY constructs its own for each density field it ray traces. We augment the standard oct-tree by associating with every cell an axis-aligned bounding box (AABB) that is just large enough to encompass the smoothing lengths of all the particles in that cell (Figure 1).

Each cell of our tree contains either particles or daughter cells. The maximum number of particles in a leaf is specified in a configuration file. We have found 12 to be a reasonable choice. The search for particle-ray intersections proceeds exactly as in the case of a simple SPH neighbor search. Starting with the root cell, the AABB of the cells are tested for intersection with the ray. In case of intersection, the cell

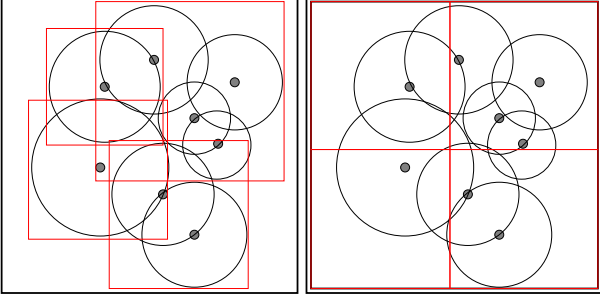


**Figure 1.** Cartoon 2D representation of several SPH particles. The left panel shows the positions of the axis aligned bounding boxes and the right panel indicates the quad-tree cell boundaries.

is opened and the search proceeds on the daughter cells. This process continues until a leaf with no further refinements is encountered, in which case the particles in the leaf are tested to see which of them are intersected by the ray. This also produces the impact parameters of each particle in the raylist.

The intersection test of the ray with the AABB is done using plücker coordinates (Mahovsky & Wyvill, 2004), a very fast method used in computer graphics. This method tests the ray against the edges comprising the silhouette of the AABB instead of testing against the individual faces, it is division free and consists of a number of simple dot-product operations.

### 3.5 Solvers

Once we have a photon packet and a list of the ray-particle intersections stored in a raylist, we can proceed to update all the particles in the raylist. SPHray offers two choices for this task. The first is an adaptive Runge-Kutta (RK) method. A set of formulas due to Fehlberg (1970) provide solutions that are accurate to fifth order in the time step. Step size control is provided using the truncation error as estimated by the embedded fourth order solution. The Cash-Karp coefficients Cash & Karp (1990) are used to take the variable length time steps. This option is included because it is simple and could be easily modified if a user needs to add extra physics into the solution routine. It is also guaranteed to conserve photons to an arbitrary accuracy by forcing the number of ionizations in a particle to equal the number of photons removed from a packet.

The second solution method is an iterative solver based on time averaged photoionization rates and optical depths. The time averaging removes the need for very short time steps, but requires approximate analytic solutions and in the case of extremely long time steps will not conserve photons exactly. The main advantage is that the number of iterations necessary to obtain a converged solution can be much smaller than the number of RK time steps necessary to obtain the same solution. This method was introduced in Mellema et al. (2006) and a more detailed description of it can be found there.

#### 3.5.1 Runge-Kutta

For each intersection we determine the time  $t_{li}$  since the particle has last been intersected by a ray. The photon flux  $\dot{N}_\gamma$  at the particle is estimated as the photons left in the ray  $N_l$  divided by  $t_{li}$ . This is taken to be the first guess for a time step in the solution of the system of coupled differential equations (Eqs. 15,17,18, and 52). The optical depth through the particle is estimated using the technique described in §3.2. This allows the calculation of the total photoionization rate  $\Gamma$  which along with the values of  $G_A$  and  $R_I$  are all that is necessary to calculate the right hand sides of the equations mentioned above. The photoionization rate is

$$\Gamma = \dot{N}_\gamma (1 - e^{-\Delta\tau}) \times \frac{m_H}{M_p} \left[ X x_{\text{HI}} + \frac{Y}{4} (x_{\text{HeI}} + x_{\text{HeII}}) \right]^{-1} \quad (73)$$

where  $\dot{N}_\gamma$  is the photon flux at the particle,  $\Delta\tau$  is the optical depth through the particle,  $m_H$  is the mass of a Hydrogen atom,  $M_p$  is the mass of the particle,  $X$  is the Hydrogen mass fraction and  $Y$  is the Helium mass fraction. Here,  $x_{\text{HeI}}$  and  $x_{\text{HeII}}$  should be set to zero for frequencies less than their respective thresholds.  $\Gamma$  for the individual species is calculated from the ratio of their optical depths to the total optical depth.

$$\Gamma_A = \frac{\Delta\tau_A}{\Delta\tau} \quad (74)$$

The number of photons absorbed by a particle  $N_a$  is obtained by solving an extra differential equation, as the photoionization rate is allowed to vary for each substep that the RK routine takes.

The photon packet is followed along a ray until the fraction of photons left is below a threshold or until the photon packet has reached a pre-determined distance along the ray. A typical value for the photon tolerance is  $1.0 \times 10^{-10}$  of the initial photons in the packet. This determines the level of photon conservation and can be set arbitrarily low.

#### 3.5.2 Iterative

If the iterative solution method is chosen, the default time step  $t_{li}$  can be used for most updates. The first step in this solution method is to initialize the time averaged ionization fractions to the current values in a particle. These are used to make a first guess at the time averaged optical depth and photoionization rate.

$$\langle \Gamma \rangle = \dot{N}_\gamma (1 - e^{-\langle \Delta\tau \rangle}) \times \frac{m_H}{M_p} \left[ X \langle x_{\text{HI}} \rangle + \frac{Y}{4} (\langle x_{\text{HeI}} \rangle + \langle x_{\text{HeII}} \rangle) \right]^{-1} \quad (75)$$

This time averaged photoionization rate is used to calculate the time averaged ionization fractions (Eqs. 52-56) which are in turn used to update the time averaged optical depths. The optical depths can then be used to find a new photoionization rate and the iteration proceeds until we have reached convergence in the electron number density and temperature. Because the heating and cooling rates are themselves functions of temperature (as opposed to the recombination and collisional ionization rates which are not functions of the ionization fraction), the temperature is always updated using the RK routine and the ionization state



at each iteration. Once the iterations have converged, the final state of the particle is calculated using eqs. 28 - 32.

## 4 CODE VERIFICATION

Here we present the results of SPHRAY on the tests outlined in the radiative transfer comparison project paper by Iliev et al. (2006). We will describe the tests briefly, but refer the reader to the reference for details. For tests 1 and 2, the initial conditions were set up using SPH particles that were evolved into a glass state using the code GADGET-2 (Springel, 2005). The distribution of particles extended two smoothing lengths further than the required box size in order to avoid edge effects in the density field and vacuum boundary conditions were used.

Tests 1 and 2 contained exactly  $128^3$  SPH particles within the  $6.6^3 \text{ kpc}^3$  volume while test 3 contained 2,135,842 particles in this same volume. For the third test, 853,442 particles were first evolved into a glass and then SPH particles were randomly placed inside the clump until the density there had reached 200 times the density outside the clump. The initial conditions for the cosmological test are discussed in §4.1.4. The SPH density field as well as the temperature and ionization fraction variables have been interpolated onto a  $128^3$  grid to make the surface plots and for submission to the Comparison Project website and so for those figures we will refer to grid cells.

### 4.1 Test 1. Pure hydrogen isothermal H II region expansion

The first test considers the growth of a Strömgren sphere in a uniform density field consisting of pure hydrogen. The source, placed in the corner of a  $6.6 \text{ kpc}$  box, emits  $\dot{N}_\gamma = 5.0 \times 10^{48}$  Rydberg photons per second. The density of hydrogen is  $n_{\text{H}} = 1.0 \times 10^{-3} \text{ cm}^{-3}$ , and the temperature is fixed at  $T = 10,000 \text{ K}$ . The system is evolved for 500 Myr or approximately four recombination times. The state of the system is examined at 10 and 100 Myr when the I-front is growing quickly and at 500 Myr when the photoionizations and recombinations have balanced and the HII region has reached its final Strömgren radius.

This simple test has the advantage that numerical results can be compared directly with an analytic solution for the position and velocity of the I-front versus time. SPHRAY finds agreement with these solutions at the several percent level (Figure 3). The analytic front width, defined as the distance over which the neutral fraction goes from  $x_{\text{HI}} = 0.1$  to  $x_{\text{HI}} = 0.9$  is  $r_{\text{if}} \approx 18\lambda_{\text{mfp}} \approx 14$  grid cells (Iliev et al., 2006) and is also reproduced by SPHRAY. This can be seen in figure 2, by noting that the contours are at  $x_{\text{HI}} = 0.1$  and  $x_{\text{HI}} = 0.9$ .

The size of the highly ionized proximity region produced by all the codes in the comparison project can be seen by examining the neutral fraction lines in figure 3. Our solution follows closely that produced by RSPH. There are several codes that produce slightly smaller proximity regions than the rest. These codes may not have converged or be unable to reach the native resolution of the density field as SPHRAY produced similar results before converging as can be seen in figure 4.

The anisotropies seen in the surface plots of SPHRAY's results have three major sources: the Monte Carlo method used, Poisson fluctuations in the sampling of solid angle by the rays, and fluctuations in the density field due to the SPH glass. In future work, it may be useful to use a low discrepancy sequence instead of uniformly distributed pseudo random numbers to generate ray directions, however given the fact that these anisotropies can be reduced by tracing more rays and the agreement of the radially averaged profiles we consider this a minor problem.

### 4.2 Test 2. HII region expansion: the temperature state

Test 2 is identical to Test 1 except the gas temperature is now allowed to vary, starting from an initial value of  $T = 100 \text{ K}$  and the spectrum of the ionizing source is taken to be that of a  $T = 10^5 \text{ K}$  blackbody. This is a more demanding test as the heating times are very short in comparison with the other characteristic times and now the rays must sample frequency space as well. Multi-frequency photon packets would alleviate the need for this extra sampling and are planned as an additional option in future versions of SPHRAY.

The radially averaged ionization (figure 7) and temperature (figure 8) profiles that SPHRAY produced for this test again follow very closely those produced by RSPH. SPHRAY correctly produces a preheated region ahead of the ionization front due to the accurate treatment of high energy photons with long mean free paths and a large amount of energy to deposit as heat.

### 4.3 Test 3. I-front trapping in a dense clump and the formation of a shadow

In this test, a cold dense spherical clump of hydrogen gas is embedded in a hot diffuse background. The dimensions of the simulation box are the same as above ( $6.6^3 \text{ kpc}^3$ ). The clump has a radius  $r_c = 0.8 \text{ kpc}$  and its center is located at,  $x_c = (5.0, 3.3, 3.3) \text{ kpc}$ . The density contrast is  $n_{\text{in}}/n_{\text{out}} = 200$  with  $n_{\text{out}} = 2 \times 10^{-4} \text{ cm}^{-3}$ . The gas in the clump is set to a temperature of  $T_{\text{in}} = 40 \text{ K}$  while the gas outside the clump is initialized to  $T_{\text{out}} = 8000 \text{ K}$ . The entire  $x = 0$  side of the simulation box is taken to be a  $T = 10,000 \text{ K}$  blackbody source with a constant photon flux,  $F = 10^6 \text{ s}^{-1} \text{ cm}^{-2}$  into the box. The test is designed so that the initially fast moving ionization front will be trapped in the clump due to the higher recombination rate there.

In figures 9 and 10 we show the ionization and temperature profiles along a small cylinder through the axis of symmetry. For the Comparison Project grid data, we used the four central columns of grid cells (where each grid cell is  $\approx 0.05 \text{ kpc}$  in length) and for our SPH data we used all the particles whose centers lie within  $0.05 \text{ kpc}$  of the axis of symmetry. The variation between all the codes is larger for this test than the first two. SPHRAY produces results that lie between those of RSPH and CRASH for the ionization profiles and results that follow RSPH for the temperature profiles.

This test features many of the effects that contribute to a reprocessing of the intergalactic background radiation

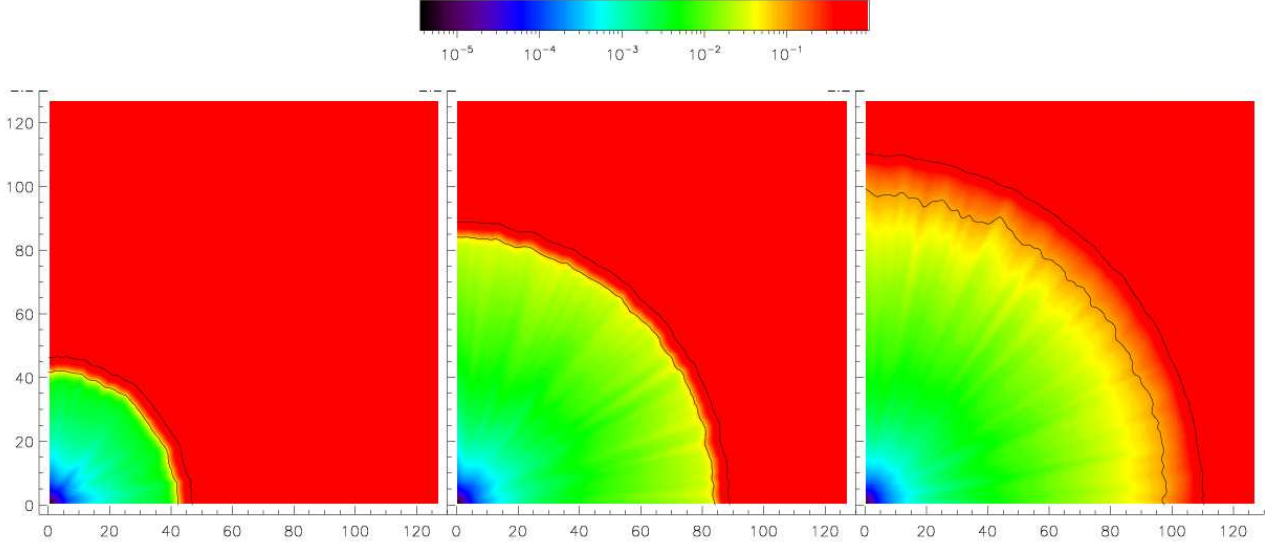


**Figure 2.** Comparison Project Test 1 (HII region expansion in a gas at constant density and temperature). Surface plot of  $x_{\text{HI}}$  cut through the simulation volume at coordinate  $z = 0$  at  $t = 10$  (left), 30 (middle), and 500 (right) Myr. The contours are at  $x_{\text{HI}} = 0.1$  and  $x_{\text{HI}} = 0.9$ . The number of rays traced  $N_t$  by SPHRAY is  $q \times 10^8$  where  $q = t/500$  is the fraction of elapsed time. The axes are measured in grid cells.

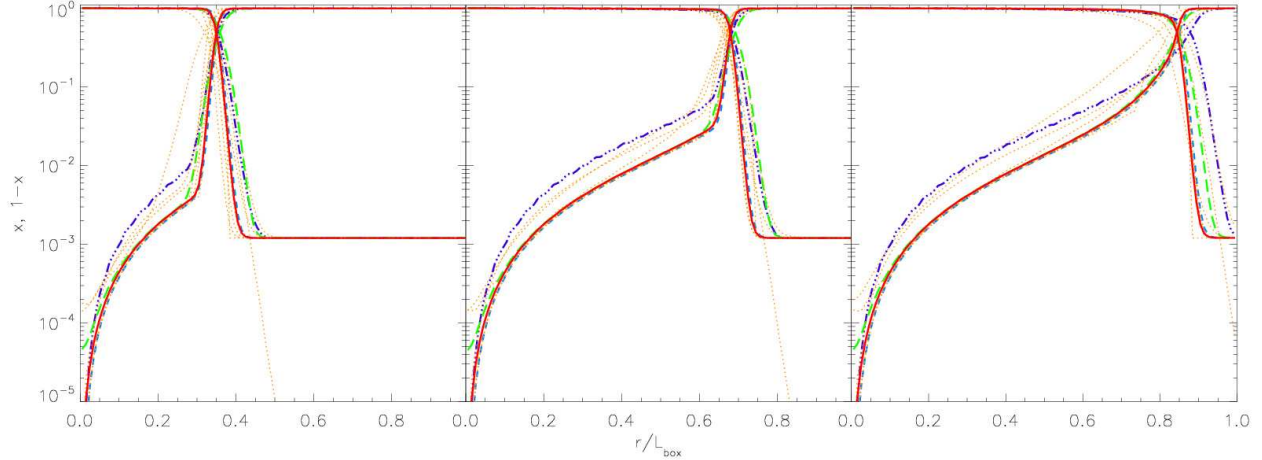


**Figure 3.** Comparison Project Test 1 (HII region expansion in a gas at constant density and temperature).  $x_{\text{HI}}$  and  $x_{\text{HII}}$  radial profiles at  $t = 10$  (left), 100 (middle), and 500 (right) Myr. The number of rays traced  $N_t$  by SPHRAY is  $q \times 10^7$  where  $q = t/500$  is the fraction of elapsed time. Shown are the results from SPHRAY (solid red line), CRASH (dash-dot-dot-dot purple line), RSPH (dashed green line), C<sup>2</sup>-Ray (small dashed light blue line) and the results from all the other codes in the comparison project that completed this test (dotted orange lines).

field. Specifically, self shielding, shadowing, and spectral hardening. SPHRAY produces an ionization front that moves quickly to the clump and is trapped near the center as it should be. The differences with the other codes mostly have to do with the amount of shadowing and self shielding (ionization and temperature). The high energy photons that are sampled by SPHRAY produce slightly weaker shadows directly behind the clump than most of the other codes. The results are much more pronounced for the temperature than

they are for ionization. In the last panel of figure 11 the self shielded section of the clump and the area in the shadow of the clump are only slightly ionized, however in the last panel of figure 12 the high energy photons have raised the temperature of the whole initially cool clump to  $\approx 10,000$  K and begun to heat the shadowed region behind it above its initial temperature of 8,000 K,

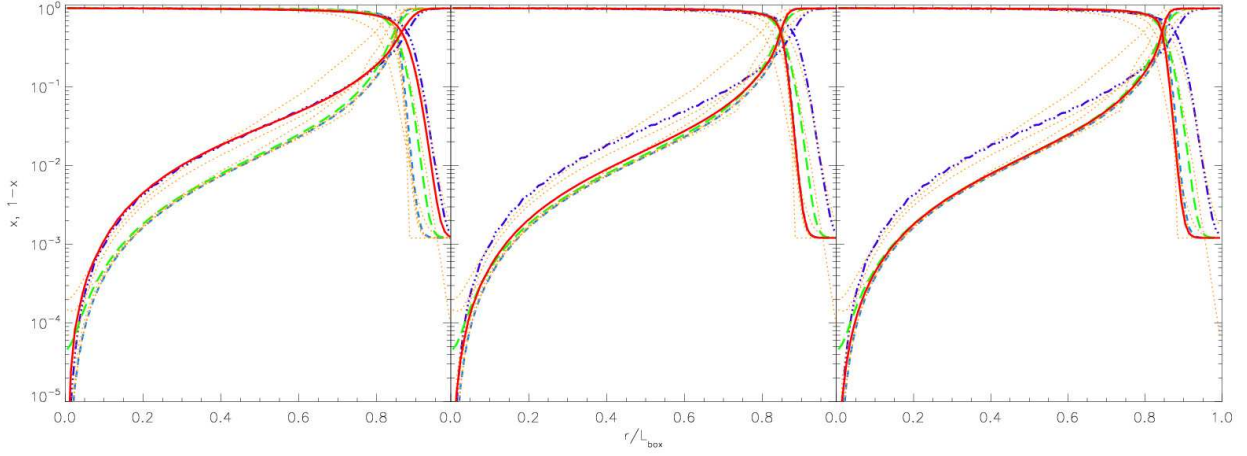


**Figure 4.** Comparison Project Test 1 (HII region expansion in a gas at constant density and temperature).  $x_{\text{HI}}$  and  $x_{\text{HII}}$  radial profiles at  $t = 10$  Myr with  $N_t = q \times 10^6$  (left),  $N_t = q \times 10^7$  (middle), and  $N_t = q \times 10^8$  (right) where  $N_t$  is the number of rays traced and  $q = 10/500$  is the fraction of elapsed time. Shown are the results from SPHRAY (solid red line), CRASH (dash-dot-dot-dot purple line), RSPH (dashed green line), C<sup>2</sup>-Ray (small dashed light blue line) and the results from all the other codes in the comparison project that completed this test (dotted orange lines).

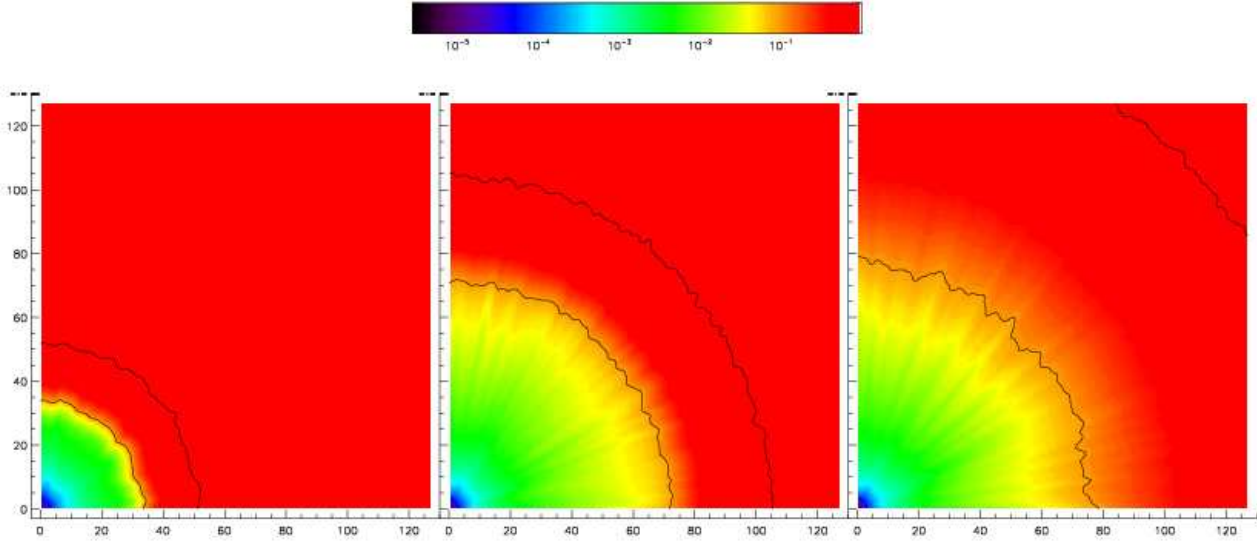


**Figure 5.** Comparison Project Test 2 (HII region expansion in a gas at constant density with varying temperature). Surface plot of  $x_{\text{HI}}$  cut through the simulation volume at coordinate  $z = 0$  and  $t = 10$  (left), 100 (middle), and 500 (right) Myr. The contours are at  $x_{\text{HI}} = 0.1$  and  $x_{\text{HI}} = 0.9$ . The number of rays traced  $N_t$  by SPHRAY is  $q \times 10^8$  where  $q = t/500$  is the fraction of elapsed time. The axes are measured in grid cells.

#### 4.4 Test 4. Multiple sources in a cosmological density field

The most realistic test performed in the RT comparison project involved sources placed in the 16 most massive halos of a cosmological simulation snapshot at  $z=9$ . The box size is  $0.5 h^{-1}$  comoving Mpc and the gas was initially neutral with a temperature of 100 K. The sources were assumed to

emit  $f_\gamma = 250$  photons per atom over  $t_s = 3$  Myr leading to a photon flux  $\dot{N}_\gamma$  of,

$$\dot{N}_\gamma = f_\gamma \frac{M \Omega_b}{\Omega_0 m_H t_s}. \quad (76)$$

where  $M$  is the halo mass. The system was then evolved for 0.4 Myr.

In order for SPHRAY to complete this test it was necessary to convert the density field data from a grid based rep-

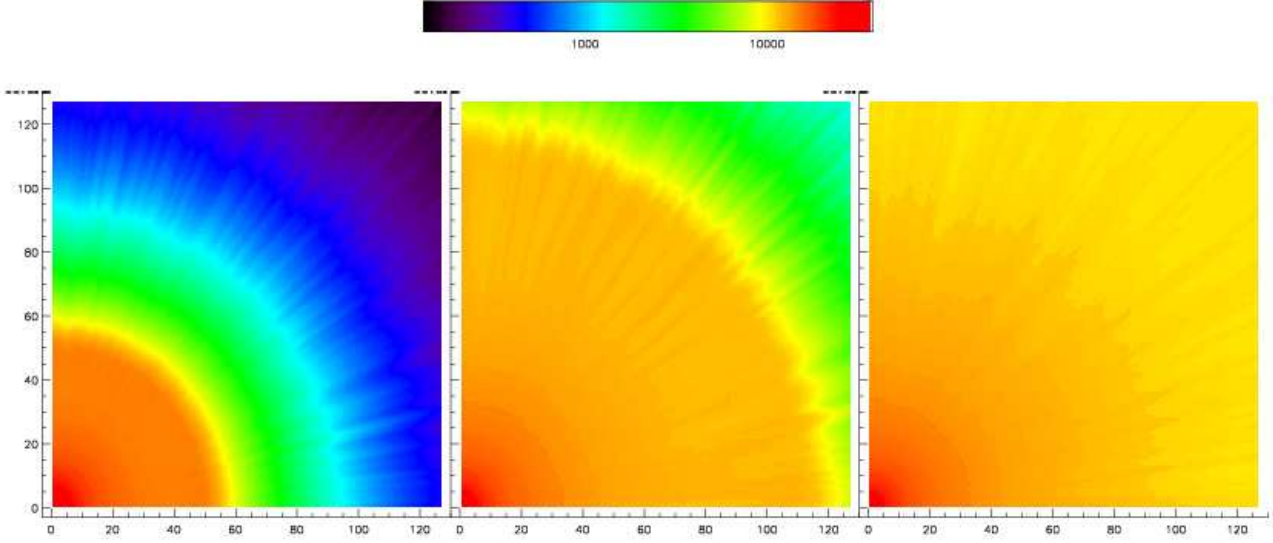


**Figure 6.** Comparison Project Test 2 (HII region expansion in a gas at constant density with varying temperature). Surface plot of the temperature cut through the simulation volume at coordinate  $z = 0$  and  $t = 10$  (left), 100 (middle), and 500 (right) Myr. The number of rays traced  $N_t$  by SPHRAY is  $q \times 10^8$  where  $q = t/500$  is the fraction of elapsed time. The axes are measured in grid cells.

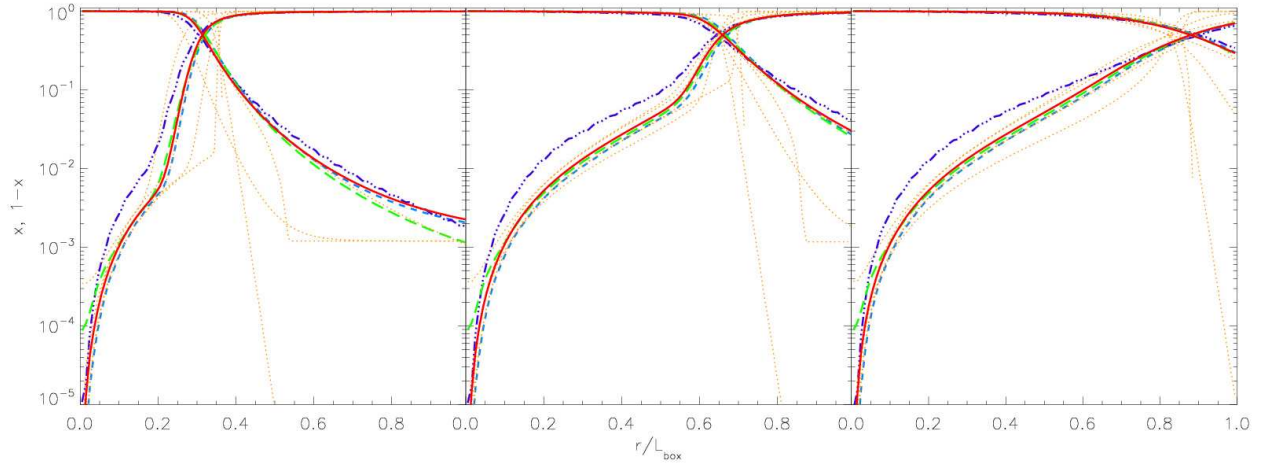


**Figure 7.** Comparison Project Test 2 (HII region expansion in a gas at constant density with varying temperature). Spherically averaged  $x_{\text{HI}}$  and  $x_{\text{HII}}$  profiles at  $t = 10$  (left), 100 (middle), and 500 (right) Myr. The number of rays traced  $N_t$  by SPHRAY is  $q \times 10^7$  where  $q = t/500$  is the fraction of elapsed time. Shown are the results from SPHRAY (solid red line), CRASH (dash-dot-dot-dot purple line), RSPH (dashed green line),  $C^2$ -Ray (small dashed light blue line) and the results from all the other codes in the comparison project that completed this test (dotted orange lines).

resentation into an SPH density field. This was accomplished using the following procedure: we start from a smooth glass distribution representing a constant density field equal to the peak density  $\rho_{\text{max}}$  of the grid data. Particles are then selected for removal according to a comparison of the density  $\rho_p$  at the particle position with a random density  $\rho_X$  where  $0 < \rho_X < \rho_{\text{max}}$ . This gives a density field which is smoother in high density regions than it would be if a normal acceptance-rejection test with random particle locations

was used. In low density regions the noise is higher because the distribution becomes less glass like as particles are removed. The result was a close approximation to the gridded density field using 1,957,344 SPH particles. The test does show some extraneous noise from the conversion to particles, but this noise is smaller than the difference between different methods so for our comparison, the simple procedure outlined above was good enough. SPHRAY is intended

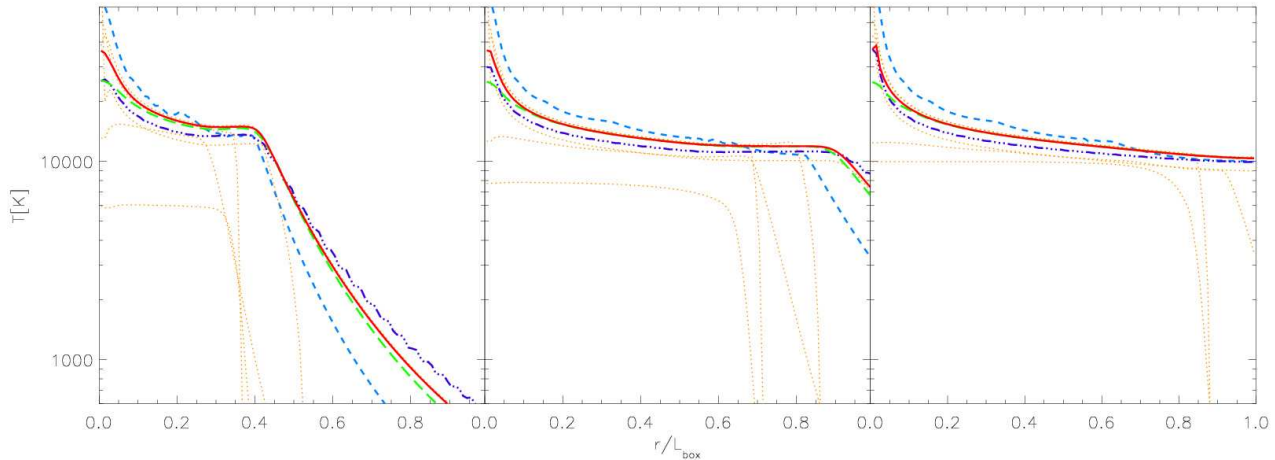


**Figure 8.** Comparison Project Test 2 (HII region expansion in a gas at constant density with varying temperature). . Spherically averaged temperature profiles at  $t = 10$  (left), 100 (middle), and 500 (right) Myr. The number of rays traced  $N_t$  by SPHRAY is  $q \times 10^7$  where  $q = t/500$  is the fraction of elapsed time. Shown are the results from SPHRAY (solid red line), CRASH (dash-dot-dot-dot purple line), RSPH (dashed green line), C<sup>2</sup>-Ray (small dashed light blue line) and the results from all the other codes in the comparison project that completed this test (dotted orange lines).

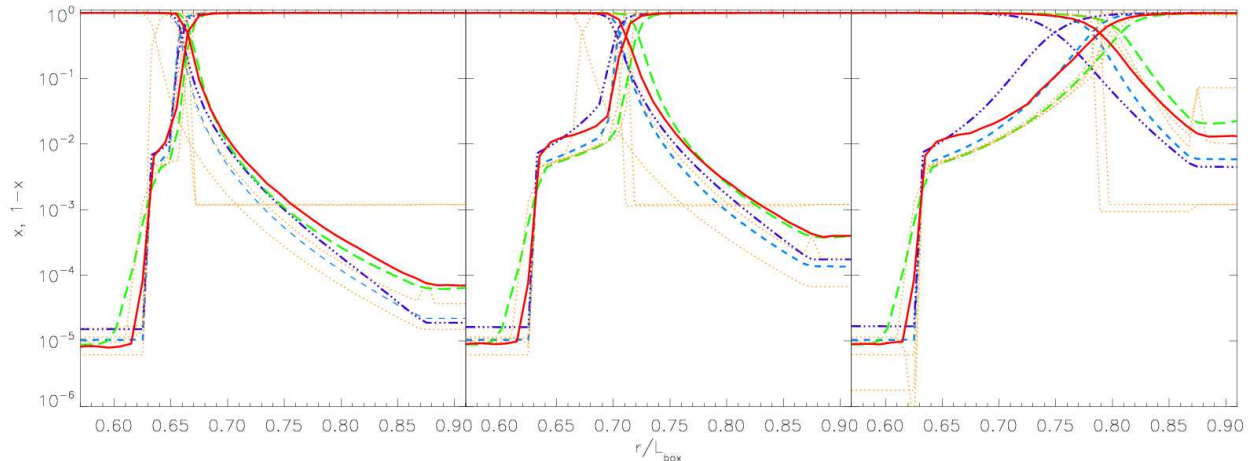


**Figure 9.** Comparison Project Test 3 (I-front trapping in a dense clump).  $x_{\text{HI}}$  and  $x_{\text{HII}}$  profiles along the axis of symmetry at  $t = 1$  (left), 3 (middle), and 15 (right) Myr. The number of rays traced  $N_t$  by SPHRAY is  $q \times 10^8$  where  $q = t/15$  is the fraction of elapsed time. Shown are the results from SPHRAY (solid red line), CRASH (dash-dot-dot-dot purple line), RSPH (dashed green line), C<sup>2</sup>-Ray (small dashed light blue line) and the results from all the other codes in the comparison project that completed this test (dotted orange lines).

to be run on density fields produced by SPH hydrodynamic simulations in which this sort of noise would not occur.

The results from SPHRAY are compared with those of C<sup>2</sup>-Ray (Mellema et al., 2006), FTTE (Razoumov & Cardall, 2005), and CRASH (Maselli et al., 2003) in figures 13 to 16. General features of the ionization field including the extent and shape of the ionization front, the shadows from dense clumps, and the shape of the neutral island near the center of the slice, are similar in all codes. Although SPHRAY and CRASH share the most similarities, including the sampling of high energy photons, we see some slight differences in the

peak ionization and temperature values they produce in the central part of the highly ionized region.

## 5 DISCUSSION

We have presented the cosmological SPH raytracing code SPHRAY and discussed the results of several radiative transfer problems by way of validation. SPHRAY employs a Monte Carlo approach to ray tracing applied directly to the SPH particle distribution native to a large fraction of current astrophysical and cosmological hydrodynamic simulations.



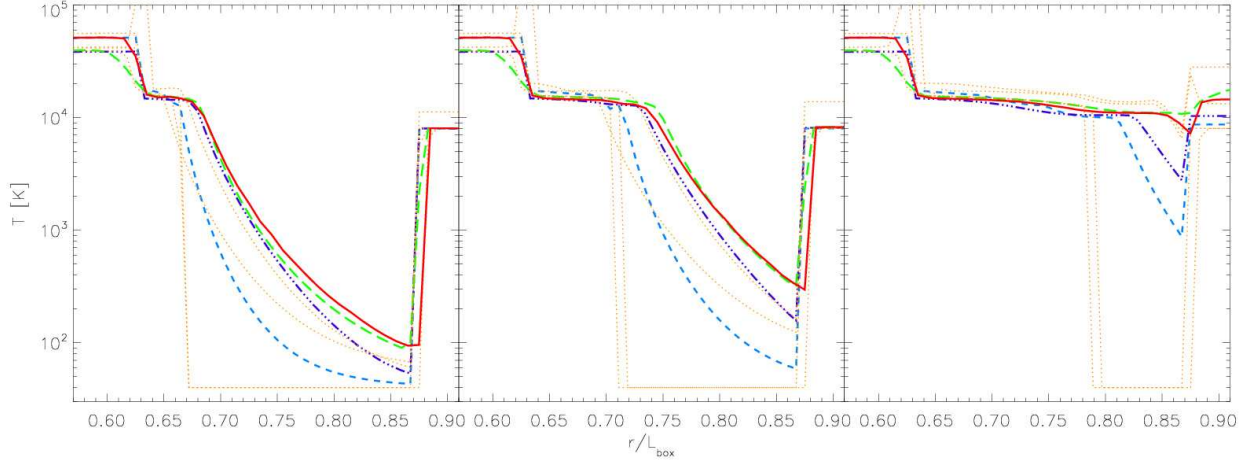


**Figure 10.** Comparison Project Test 3 (I-front trapping in a dense clump). Temperature profiles along the axis of symmetry at  $t = 1$  (left), 3 (middle), and 15 (right) Myr. The number of rays traced  $N_t$  by SPHray is  $q \times 10^8$  where  $q = t/15$  is the fraction of elapsed time. Shown are the results from SPHray (solid red line), CRASH (dash-dot-dot-dot purple line), RSPH (dashed green line), C<sup>2</sup>-Ray (small dashed light blue line) and the results from all the other codes in the comparison project that completed this test (dotted orange lines).

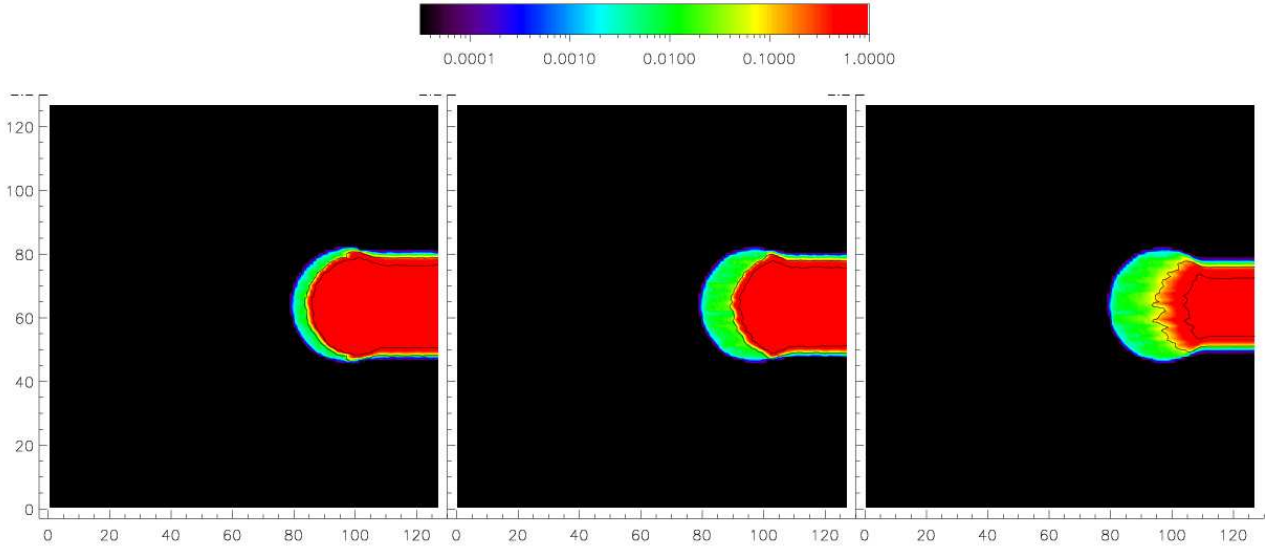


**Figure 11.** Comparison Project Test 3 (I-front trapping in a dense clump). Surface cut of the neutral fraction at  $t = 1$  (left), 3 (middle), and 15 (right) Myr. The number of rays traced  $N_t$  by SPHray is  $q \times 10^8$  where  $q = t/15$  is the fraction of elapsed time. Shown are the results from SPHray

The column density sums at the heart of the radiative transfer calculation are carried out using the SPH kernels so that no regridding of the data is necessary, maintaining the adaptive Lagrangian nature that makes SPH attractive in the first place. The statistical nature of the Monte Carlo method makes the inclusion of arbitrary source spectra and emission profiles very straightforward. The simplicity of its implementation also allows the future addition of more complicated physics as well as parallelization. However, a large number of rays must be traced to get a fair representation of the

underlying probability distribution functions being sampled and to maintain angular resolution. This translates to the numerical problem of finding the intersection of numerous rays and spheres as quickly as possible. In order to do this we have applied a variant of the neighbor search techniques using oct-trees and a fast box-ray intersection test adapted from computer graphics, resulting in an efficient adaptive ray tracing code applicable to current astronomical hydro simulations.

There are, in general, no analytic solutions to the

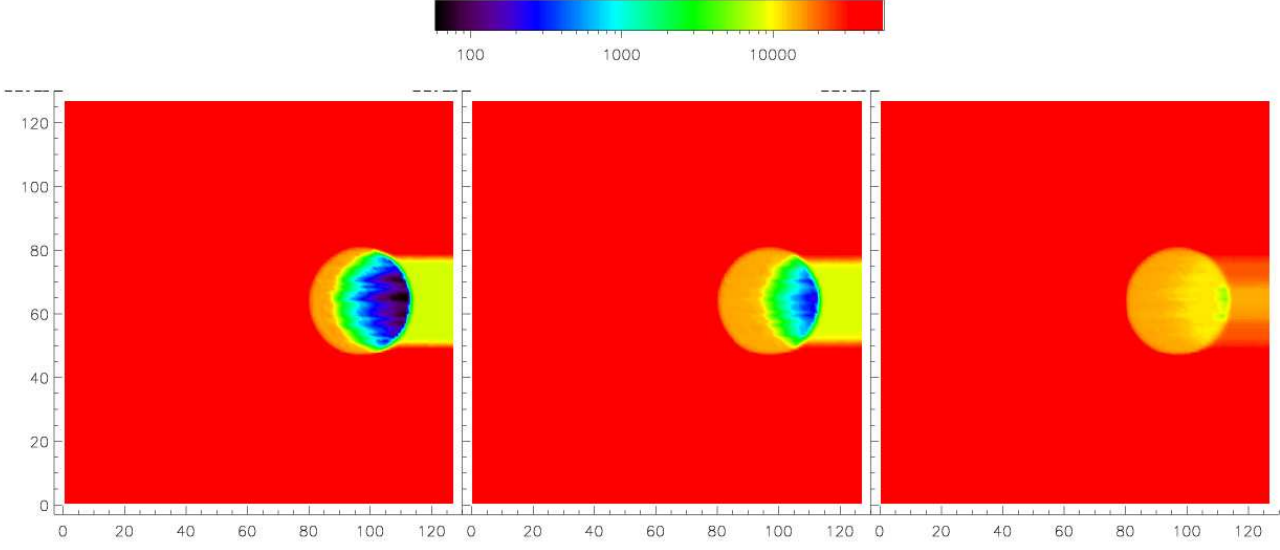


**Figure 12.** Comparison Project Test 3 (I-front trapping in a dense clump). Surface cut of the temperature at  $t = 1$  (left), 3 (middle), and 15 (right) Myr. The number of rays traced  $N_t$  by SPHRAY is  $q \times 10^8$  where  $q = t/15$  is the fraction of elapsed time. Shown are the results from SPHRAY

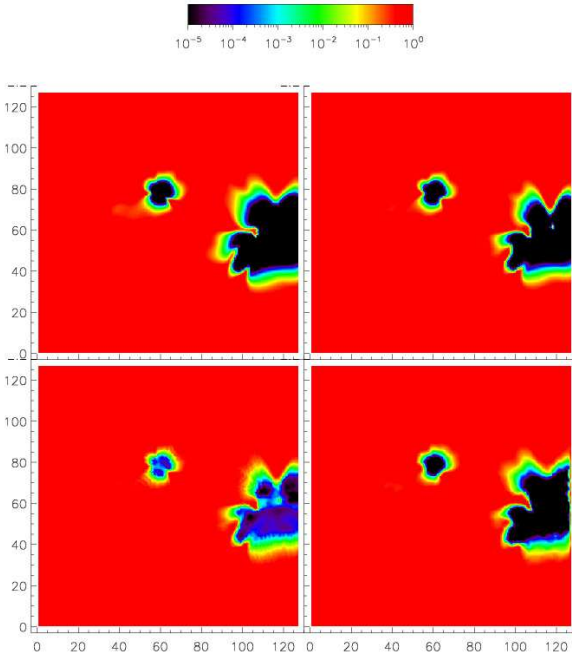


**Figure 13.** Comparison Project Test 4 (Multiple sources in a cosmological density field). Surface cut of the neutral fraction through the middle of the simulation volume at  $t = 0.05$  Myr. The number of rays traced  $N_t$  by SPHRAY is  $q \times 10^8$  where  $q = t/0.4$  is the fraction of elapsed time. Beginning in the top left corner and proceeding clockwise are the results from C<sup>2</sup>-Ray, FTTE, SPHRAY, and CRASH.

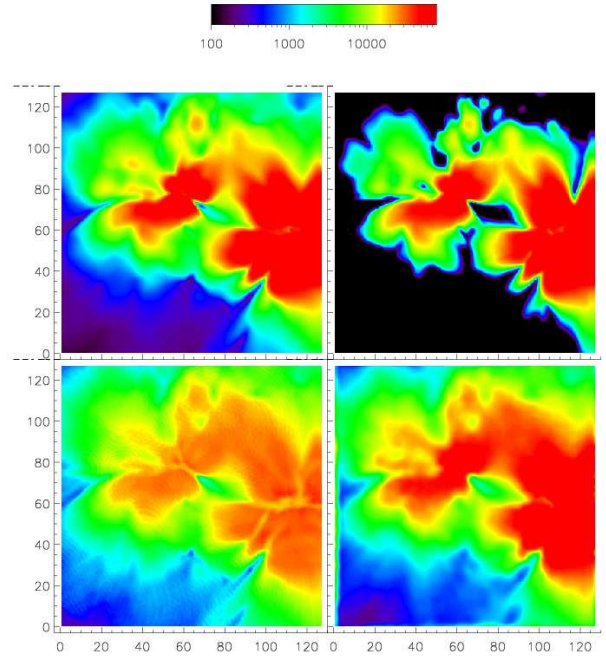


**Figure 14.** Comparison Project Test 4 (Multiple sources in a cosmological density field). Surface cut of the temperature through the middle of the simulation volume at  $t = 0.05$  Myr. The number of rays traced  $N_t$  by SPHRAY is  $q \times 10^8$  where  $q = t/0.4$  is the fraction of elapsed time. Beginning in the top left corner and proceeding clockwise are the results from C<sup>2</sup>-Ray, FTTE, SPHRAY, and CRASH.

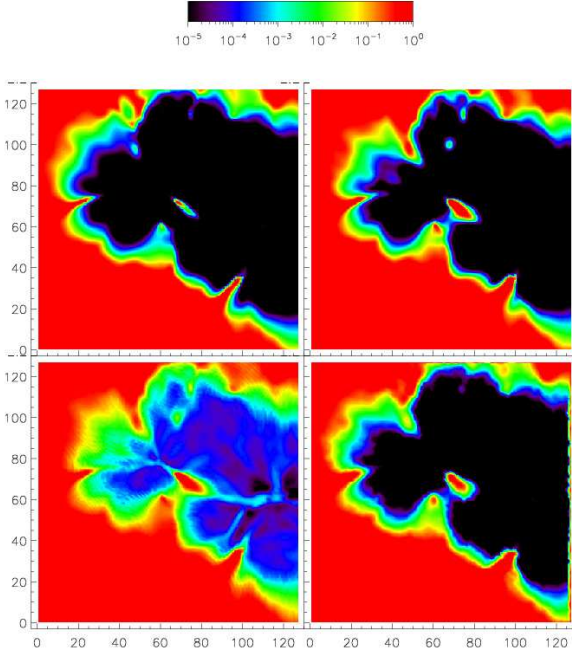


**Figure 15.** Comparison Project Test 4 (Multiple sources in a cosmological density field). Surface cut of the neutral fraction through the middle of the simulation volume at  $t = 0.2$  Myr. The number of rays traced  $N_t$  by SPHRAY is  $q \times 10^8$  where  $q = t/0.4$  is the fraction of elapsed time. Beginning in the top left corner and proceeding clockwise are the results from C<sup>2</sup>-Ray, FTTE, SPHRAY, and CRASH.

types of radiative transfer problems that occur with sources embedded in 3D density fields. Therefore we validated SPHRAY using the tests chosen by the Radiative Transfer Comparison Project. There is good agreement of SPHRAY results with codes that treat the same level of physics.

We present the source code for SPHRAY on a companion website<sup>9</sup>, together with a users guide and some example input snapshot files. An early version of this RT approach was used to study the structure of neutral hydrogen in the Universe at the time of reionization in Croft & Altay (2007).

## ACKNOWLEDGMENTS

This project is supported by the National Science Foundation, NSF AST-0205978 and by NASA ATP grant NNG 06-GH88G. We thank Intel for their generous donation of processors used in this work.

## APPENDIX A: PHOTO-IONIZATION CROSS-SECTIONS AND ATOMIC COOLING/HEATING RATES

The rates below make use of the following notation,

<sup>9</sup> <http://www.sphray.org>

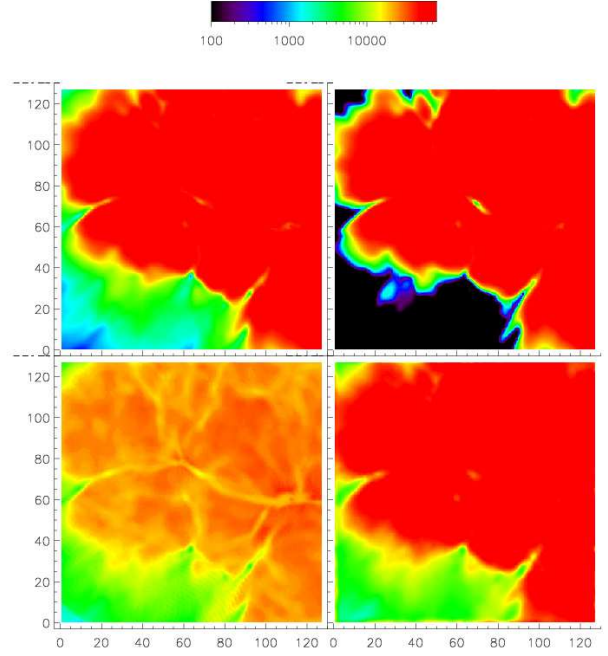


**Figure 16.** Comparison Project Test 4 (Multiple sources in a cosmological density field). Surface cut of the temperature through the middle of the simulation volume at  $t = 0.2$  Myr. The number of rays traced  $N_t$  by SPHRAY is  $q \times 10^8$  where  $q = t/0.4$  is the fraction of elapsed time. Beginning in the top left corner and proceeding clockwise are the results from C<sup>2</sup>-Ray, FTTE, SPHRAY, and CRASH.

$$\lambda_A = 2 \frac{T_A}{T} \quad (\text{A1})$$

where the  $T_A$  are the ionization energies of the photo absorbing species in temperature units,

$$T_{\text{HI}} = 157,809\text{K} \quad (\text{A2})$$

$$T_{\text{HeI}} = 285,335\text{K} \quad (\text{A3})$$

$$T_{\text{HeII}} = 631,515\text{K} \quad (\text{A4})$$

and,

$$T_i = \frac{T}{10^4 \text{K}} \quad (\text{A5})$$

• Recombination Rates - Case A (Hui & Gnedin, 1997) [ $\text{cm}^3 \text{s}^{-1}$ ]

$$\alpha_{\text{HII}}^A = 1.269 \times 10^{-13} \frac{\lambda_{\text{HI}}^{1.503}}{\left[1.0 + \left(\frac{\lambda_{\text{HI}}}{0.522}\right)^{0.470}\right]^{1.923}} \quad (\text{A6})$$

$$\alpha_{\text{HeII}}^A = 3.0 \times 10^{-14} \lambda_{\text{HeI}}^{0.654} \quad (\text{A7})$$

$$\alpha_{\text{HeIII}}^A = 2.538 \times 10^{-13} \frac{\lambda_{\text{HeII}}^{1.503}}{\left[1.0 + \left(\frac{\lambda_{\text{HeII}}}{0.522}\right)^{0.470}\right]^{1.923}} \quad (\text{A8})$$

• Recombination Rates - Case B (Hui & Gnedin, 1997) [ $\text{cm}^3 \text{s}^{-1}$ ]

$$\alpha_{\text{HII}}^B = 2.753 \times 10^{-14} \frac{\lambda_{\text{HI}}^{1.500}}{\left[1.0 + \left(\frac{\lambda_{\text{HI}}}{2.740}\right)^{0.407}\right]^{2.242}} \quad (\text{A9})$$



$$\alpha_{\text{HeII}}^B = 1.26 \times 10^{-14} \lambda_{\text{HeI}}^{0.750} \quad (\text{A10})$$

$$\alpha_{\text{HeIII}}^B = 5.506 \times 10^{-14} \frac{\lambda_{\text{HeII}}^{1.500}}{\left[1.0 + \left(\frac{\lambda_{\text{HeII}}}{2.740}\right)^{0.407}\right]^{2.242}} \quad (\text{A11})$$

- Collisional Ionization Rates (Cen, 1992) [ $\text{cm}^3 \text{s}^{-1}$ ]

$$\gamma_{\text{HI}} = \frac{5.85 \times 10^{-11} \sqrt{T_0}}{1 + \sqrt{T_5}} e^{-T_{\text{HI}}/T} \quad (\text{A12})$$

$$\gamma_{\text{HeI}} = \frac{2.38 \times 10^{-11} \sqrt{T_0}}{1 + \sqrt{T_5}} e^{-T_{\text{HeI}}/T} \quad (\text{A13})$$

$$\gamma_{\text{HeII}} = \frac{5.68 \times 10^{-12} \sqrt{T_0}}{1 + \sqrt{T_5}} e^{-T_{\text{HeII}}/T} \quad (\text{A14})$$

- Collisional Ionization Cooling (Cen, 1992) [ $\text{ergs cm}^{-3} \text{s}^{-1}$ ]

$$\zeta_{\text{HI}} = \frac{1.27 \times 10^{-21} \sqrt{T_0}}{1 + \sqrt{T_5}} e^{-T_{\text{HI}}/T} n_e n_{\text{HI}} \quad (\text{A15})$$

$$\zeta_{\text{HeI}} = \frac{9.38 \times 10^{-22} \sqrt{T_0}}{1 + \sqrt{T_5}} e^{-T_{\text{HeI}}/T} n_e n_{\text{HeI}} \quad (\text{A16})$$

$$\zeta_{\text{HeII}} = \frac{4.95 \times 10^{-22} \sqrt{T_0}}{1 + \sqrt{T_5}} e^{-T_{\text{HeII}}/T} n_e n_{\text{HeII}} \quad (\text{A17})$$

- Collisional Excitation Cooling (Cen, 1992) [ $\text{ergs cm}^{-3} \text{s}^{-1}$ ]

$$\psi_{\text{HI}} = \frac{7.5 \times 10^{-19}}{1 + \sqrt{T_5}} e^{-118348/T_0} n_e n_{\text{HI}} \quad (\text{A18})$$

$$\psi_{\text{HeI}} = \frac{9.10 \times 10^{-27} T_0^{-0.1687}}{1 + \sqrt{T_5}} e^{-13179/T_0} n_e^2 n_{\text{HeII}} \quad (\text{A19})$$

$$\psi_{\text{HeII}} = \frac{5.54 \times 10^{-17} T_0^{-0.397}}{1 + \sqrt{T_5}} e^{-473638/T_0} n_e n_{\text{HeII}} \quad (\text{A20})$$

- Recombination Cooling - Case A (Hui & Gnedin, 1997) [ $\text{ergs cm}^{-3} \text{s}^{-1}$ ]

$$\eta_{\text{HII}}^A = 1.778 \times 10^{-29} \frac{T_0 \lambda_{\text{HI}}^{1.965}}{\left[1.0 + \left(\frac{\lambda_{\text{HI}}}{0.541}\right)^{0.502}\right]^{2.697}} n_e n_{\text{HII}} \quad (\text{A21})$$

$$\eta_{\text{HeII}}^A = k_b T_0 \alpha_{\text{HeII}}^A n_e n_{\text{HeII}} \quad (\text{A22})$$

$$\eta_{\text{HeIII}}^A = 1.4224 \times 10^{-28} \frac{T_0 \lambda_{\text{HeII}}^{1.965}}{\left[1.0 + \left(\frac{\lambda_{\text{HeII}}}{0.522}\right)^{0.470}\right]^{1.923}} n_e n_{\text{HeIII}} \quad (\text{A23})$$

- Recombination Cooling - Case B (Hui & Gnedin, 1997) [ $\text{ergs cm}^{-3} \text{s}^{-1}$ ]

$$\eta_{\text{HII}}^B = 3.435 \times 10^{-30} \frac{T_0 \lambda_{\text{HI}}^{1.970}}{\left[1.0 + \left(\frac{\lambda_{\text{HI}}}{2.250}\right)^{0.376}\right]^{3.720}} n_e n_{\text{HII}} \quad (\text{A24})$$

$$\eta_{\text{HeII}}^B = k_b T_0 \alpha_{\text{HeII}}^B n_e n_{\text{HeII}} \quad (\text{A25})$$

$$\eta_{\text{HeIII}}^B = 2.748 \times 10^{-29} \frac{T_0 \lambda_{\text{HeII}}^{1.970}}{\left[1.0 + \left(\frac{\lambda_{\text{HeII}}}{2.250}\right)^{0.376}\right]^{3.720}} \quad (\text{A26})$$

- Bremsstrahlung Cooling (Cen, 1992) [ $\text{ergs cm}^{-3} \text{s}^{-1}$ ]

$$\beta = 1.42 \times 10^{-27} g_{ff} \sqrt{T_0} (n_{\text{HII}} + n_{\text{HeII}} + 4n_{\text{HeIII}}) n_e \quad (\text{A27})$$

where  $g_{ff} = 1.5$  is the Gaunt factor.

- Compton Heating/Cooling (Haiman et al., 1996) [ $\text{ergs cm}^{-3} \text{s}^{-1}$ ]

$$\chi = 1.017 \times 10^{-37} T_\gamma^4 (T_0 - T_\gamma) n_e \quad (\text{A28})$$

where  $T_\gamma = T_{\text{Bkgnd}}/K$  is the unitless background radiation temperature.

## REFERENCES

- Abel T., Anninos P., Zhang Y., Norman M. L., 1997, *New Astronomy*, 2, 181
- Abel T., Norman M. L., Madau P., 1999, *ApJ*, 523, 66
- Agertz O., Moore B., Stadel J., et al., 2007, *MNRAS*, 380, 963
- Anninos P., Zhang Y., Abel T., Norman M. L., 1997, *New Astronomy*, 2, 209
- Bagla J. S., 2002, *JApA*, 23, 185
- Brookshaw L., 1985, *Proceedings of the Astronomical Society of Australia*, 6, 207
- Cash J. R., Karp A. H., 1990, *ACM Trans. Math. Softw.*, 16, 3, 201
- Cen R., 1992, *ApJS*, 78, 341
- Croft R. A. C., Altay G., 2007, *arXiv:0709.2362*
- Dale J. E., Ercolano B., Clarke C. J., 2007, *MNRAS*, 382, 1759
- Di Matteo T., Colberg J., Springel V., Hernquist L., Sijacki D., 2007, *arXiv:0705.2269*
- Fehlberg E., 1970, *Computing*, 6, 61
- Frenk C. S., White S. D. M., Bode P., et al., 1999, *ApJ*, 525, 554
- Gingold R. A., Monaghan J. J., 1977, *MNRAS*, 181, 375
- Haiman Z., Thoul A. A., Loeb A., 1996, *ApJ*, 464, 523
- Heitmann K., Lukic Z., Fasel P., et al., 2007, *arXiv:0706.1270*
- Heitmann K., Ricker P. M., Warren M. S., Habib S., 2005, *ApJS*, 160, 28
- Hernquist L., Katz N., 1989, *ApJS*, 70, 419
- Hui L., Gnedin N. Y., 1997, *MNRAS*, 292, 27
- Iliev I. T., Ciardi B., Alvarez M. A., et al., 2006, *MNRAS*, 371, 1057
- Kessel-Deynet O., Burkert A., 2000, *MNRAS*, 315, 713
- Lucy L. B., 1977, *AJ*, 82, 1013
- Mahovsky J., Wyvill B., 2004, *The Journal of Graphics Tools*, 9, 1, 37
- Maselli A., Ferrara A., Ciardi B., 2003, *MNRAS*, 345, 379
- Mayer L., Lufkin G., Quinn T., Wadsley J., 2007, *ApJ*, 661, L77
- Mellema G., Iliev I. T., Alvarez M. A., Shapiro P. R., 2006, *NewA*, 11, 374
- Monaghan J. J., 1992, *ARA&A*, 30, 543
- Norman M. L., 2004, *arXiv:astro-ph/0402230*
- Norman M. L., Paschos P., Abel T., 1998, *Memorie della Societa Astronomica Italiana*, 69, 455
- O'Shea B. W., Nagamine K., Springel V., Hernquist L., Norman M. L., 2005, *ApJS*, 160, 1
- Osterbrock D. E., 1989, *Astrophysics of gaseous nebulae and active galactic nuclei*, University Science Books, Mill Valley, CA
- Oxley S., Woolfson M. M., 2003, *MNRAS*, 343, 900
- Pawlik A. H., Schaye J., 2008, *arXiv:0802.1715*
- Price D. J., 2007, *arXiv:0709.2772*
- Razoumov A., Cardall C., 2005, *MNRAS*, 362, 1413
- Regan J. A., Haehnelt M. G., Viel M., 2007, *MNRAS*, 374, 196
- Springel V., 2005, *MNRAS*, 364, 1105
- Springel V., Hernquist L., 2003, *MNRAS*, 339, 289
- Stamatellos D., Whitworth A. P., 2005, *A&A*, 439, 153
- Susa H., 2006, *PASJ*, 58, 445
- Viau S., Bastien P., Cha S. H., 2006, *ApJ*, 639, 559
- Whitehouse S. C., Bate M. R., 2004, *MNRAS*, 353, 1078
- Whitehouse S. C., Bate M. R., Monaghan J. J., 2005, *MNRAS*, 364, 1367
- Xu G., 1995, *ApJS*, 98, 355

Yoshida N., Oh S. P., Kitayama T., Hernquist L., 2007, ApJ, 663,  
687